Title
EFFECT OF MECHANICAL DISCONTINUITIES ON THE STRENGTH OF POLYCRYSTALLINE ALUMINUM OXIDE

Author
Wallace, J.S.

Publication Date
1978-09-01

EFFECT OF MECHANICAL DISCONTINUITIES ON THE STRENGTH OF POLYCRYSTALLINE ALUMINUM OXIDE

Jay S. Wallace
(M. S. thesis)

September 1978

Prepared for the U. S. Department of Energy
under Contract W-7405-ENG-48

EFFECT OF MECHANICAL DISCONTINUITIES ON THE STRENGTH OF POLYCRYSTALLINE ALUMINUM OXIDE

Jay S. Wallace

Lawrence Berkeley Laboratory
University of California
Berkeley, California 94720

ABSTRACT

This study examines the effect of artificially introduced spherical voids on the bend strength of a polycrystalline brittle solid and compares the results to traditional empirical and phenomenological porosity-strength relationships. No correlation is found between these relationships and the data.

The statistical approach by Weibull is examined particularly with regard to the implications to microstructural features. A direct test of Weibull statistics showed deviations from theory, perhaps due to the very small stressed volumes employed. Microstructural evidence suggests that some of the basic assumptions in Weibull's formulation may restrict its use in this and perhaps other systems. Based on the similarity between McClintock's Statistical model and the observed microstructural features a failure criterion for systems with randomly distributed flaws is proposed.

1. INTRODUCTION

In order for materials to be utilized to their fullest extent and greatest efficiency, correlations between microstructure and properties must be developed. Several microstructural features have been noted which affect the mechanical properties, such as, strength and fracture toughness, of brittle materials. These features include, but are by no means limited to, grain size, surface finish, microcracking and second phases. To date little analytical work has been performed relating these microstructural features to mechanical properties; most relationships have been empirical, based on bulk properties such as average grain size, mean surface finish and total second phase content.

This study is concerned with the effect of mechanical discontinuities on the fracture strength of a brittle solid. If it is assumed that the body fails from one of these introduced mechanical discontinuities, we must accurately describe the most severe flaw if we are to determine it's effect on the strength. A thorough description of the most severe flaw necessarily involves its location, shape, orientation and stress field. Because the scope of this work does not allow the time to accurately describe all of these quantities for the most general case, it is necessary to exercise caution when choosing a system for study; for this reason we have chosen to study the effects of artificially introduced, randomly distributed, spherical voids on the fracture strength of polycrystalline aluminum oxide (alumina). The variables for this system are then reduced to size-distribution and number of discontinuities.

Alumina was chosen as the matrix material for a variety of reasons. First, it is one of the most important commercial industrial ceramic materials. Second, a wealth of data exists on porosity-fracture strength relationships of commercial purity alumina. Finally, previous work in this laboratory has shown that it is possible to consistently sinter high purity alumina powder to $99.^{+}\%$ of theoretical density.

The areas in which this study differ from most previous work are in the production of voids (porosity) and purity (particularly glass phase content) of the material. Other studies have varied porosity content, as well as other microstructural features, by varying the sintering conditions. Because variations in sintering conditions change pore size- and shape-distribution as well as grain and impurity size distribution and shape, it is difficult to make an accurate evaluation of the effect of void content. Also, much of the previous materials studied had a large content (1-5%) of glassy-phase distributed along the grain boundaries. This is particularly damaging to the results since the fracture path is often intergranular rather than transgranular.

In this study the starting powder and processing conditions were identical for each specimen. Spherical voids were produced by mixing a size-separated spherical organic powder with an MgO-doped alumina starting powder, pressing, then heating the resulting green compact to burn out the organic spheres. All green compacts were then fired under identical conditions.

Four hypotheses will be proposed in section 3 to describe the fracture strength data of these specimens. The data will be presented in section 4 and compared to the hypotheses.

2. PROCEDURE

An organic material was used to produce the voids in the green compact. The following requirements were placed on the organic powder to be used in this study:

1. spherical particles
2. appreciable size fraction between 25 μm and 125 μm
3. decomposes or vaporizes below 1100°C in air
4. very low residue upon heating.

On the basis of these requirements a readily available mounting powder, Koldmount, was chosen. Thermogravimetric analysis showed that the powder burned out of a green compact at 600°C and had a 0.025% residue after heating to 900°C for 8 hours.

The organic powder was size separated in a sonic sifter using 37, 44, 63, 74, 105 and 125 μm screens. Due to electrostatic charge build-up and screen clogging all powder was screened three times before use.

The alumina powder was prepared (Fig. 2.1) by mixing 0.1 w/o MgO (as $Mg(NO_3)_2 \cdot 6H_2O$, Mallinckrodt lot XRX) and 2. w/o PVA binder (Polysciences, lot 257-8) with an isopropyl alcohol slurry of Linde A alumina powder (lot 511) in a blender for five minutes. The resulting slurry was stirred and gently heated until a mushy consistency was reached. Final drying was completed in a drying oven at 50°C. After drying, all powder was screened through a 44 μm (325 mesh) screen to break up large aggregates and to aid homogenization. A weighed amount of size separated organic was then added to the prepared alumina powder and thoroughly mixed by vigorous shaking.

Early results showed that uniform filling of the uniaxial die was necessary to prevent density gradients in the uniaxially compacted specimens that would lead to warpage upon isostatic pressing. To minimize density gradients, the uniaxial die was vibrated and evenly filled when loading powder. A minimum vibration time was used to prevent segregation of alumina powder and organic spheres. Specimens were uniaxially pressed at 15 MPa then isostatically pressed by the wet bag method at 175 MPa. The resulting green compacts had a green density of ~48% of theoretical density.

The compacts were calcined at 900°C for 8 hours to burn off the organic spheres and the PVA binder and to decompose the $Mg(NO_3)_2 \cdot 6H_2O$ to MgO.

After furnace cooling, the compacts were placed on a molybdenum pedestal and transferred to a high vacuum (10^{-6} torr) tantalum resistance Brew furnace. The firing schedule was based on previous work[15] performed in this laboratory which showed that very high density ($99.^{+}$%) could be obtained. The firing schedule was:

1. heat @ 20°C min^{-1} to 1200°C
2. heat @ 2°C min^{-1} to 1750°C
3. hold @ 1750°C for 1 hour
4. cool @ 10°C min^{-1} to room temperature.

All specimens were fired according to this schedule. After firing, the density of all specimens was measured by the Archimedes displacement method using distilled water. Void fractions were calculated from the measured density differences between samples without and with introduced voids.

Fired specimens were mounted on alumina base plates and were sawn to a 1.2 mm thickness and a width of three (3) mm using a resinoid bonded 220 grit diamond blade turning at a rim speed of ~27 m/s. The specimens were fed in the direction of blade rotation with a constant feed rate of $\sim 10^{-4}$ m/s. Flowing kerosene was used as the coolant.

Strength measurements were performed on a four point bend tester (Fig. 2.2) at an average loading rate of 4.5 $MPa \cdot sec^{-1}$. The overall span of the four point tester ($\ell_1 + \ell_2$) was 19.05 mm and the inner span (ℓ_1) was 6.35 mm. Since previous work had shown[17] that polishing the tensile surface yielded no improvement in fracture strength over the as-cut surfaces, all testing was performed with the tensile surface in the as-cut condition.

After testing, representative samples were prepared for microscopic examination. Fracture surfaces were sputtered with a 200Å gold coating to prevent charging in the SEM. Polished surfaces were prepared by polishing on 30 μm, 15 μm then 6 μm diamond bonded wheels before being lapped on 6 μm, 1 μm and finally 1/4 μm diamond impregnated nylon cloths in Syntron polishers. Since no suitable chemical etch was found, the specimens were removed from the polishing mounts and thermally etched @ 1400°C in air for four hours. The polished and etched surfaces were then sputtered with a 200Å gold coating.

Grain size was measured as the mean linear intercept of approximately 400 grains.

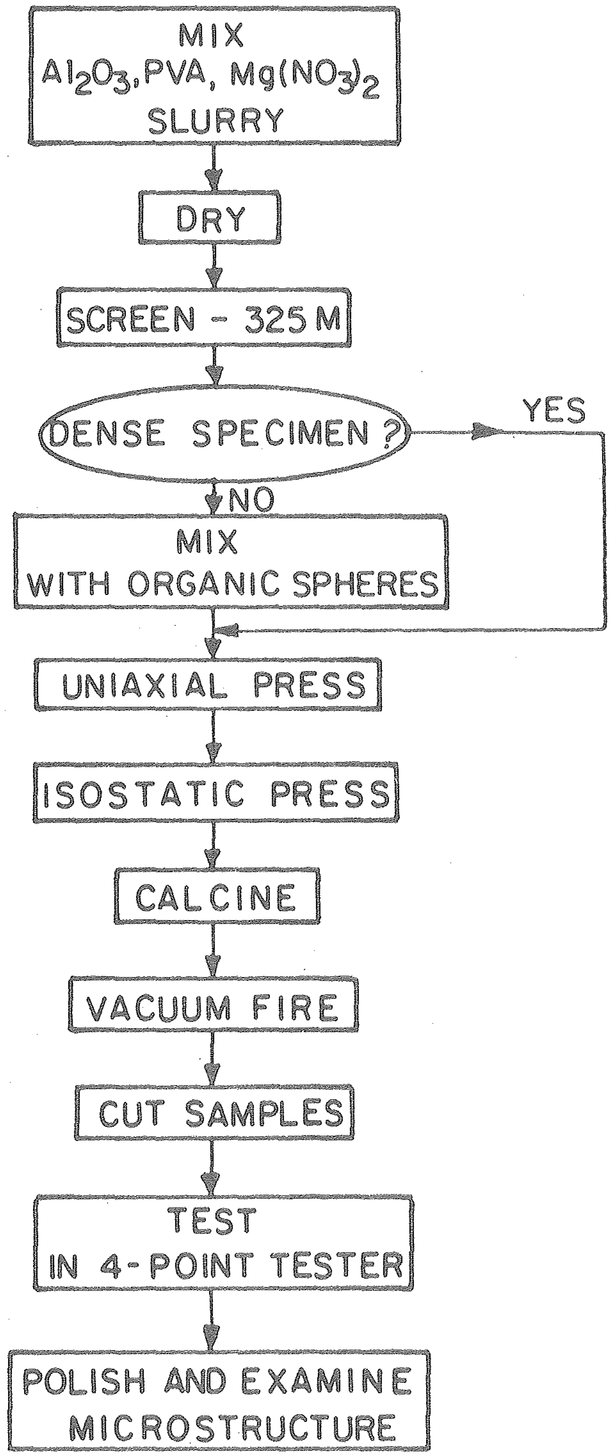

XBL789-5754

Fig. 2.1

Specimen Preparation.

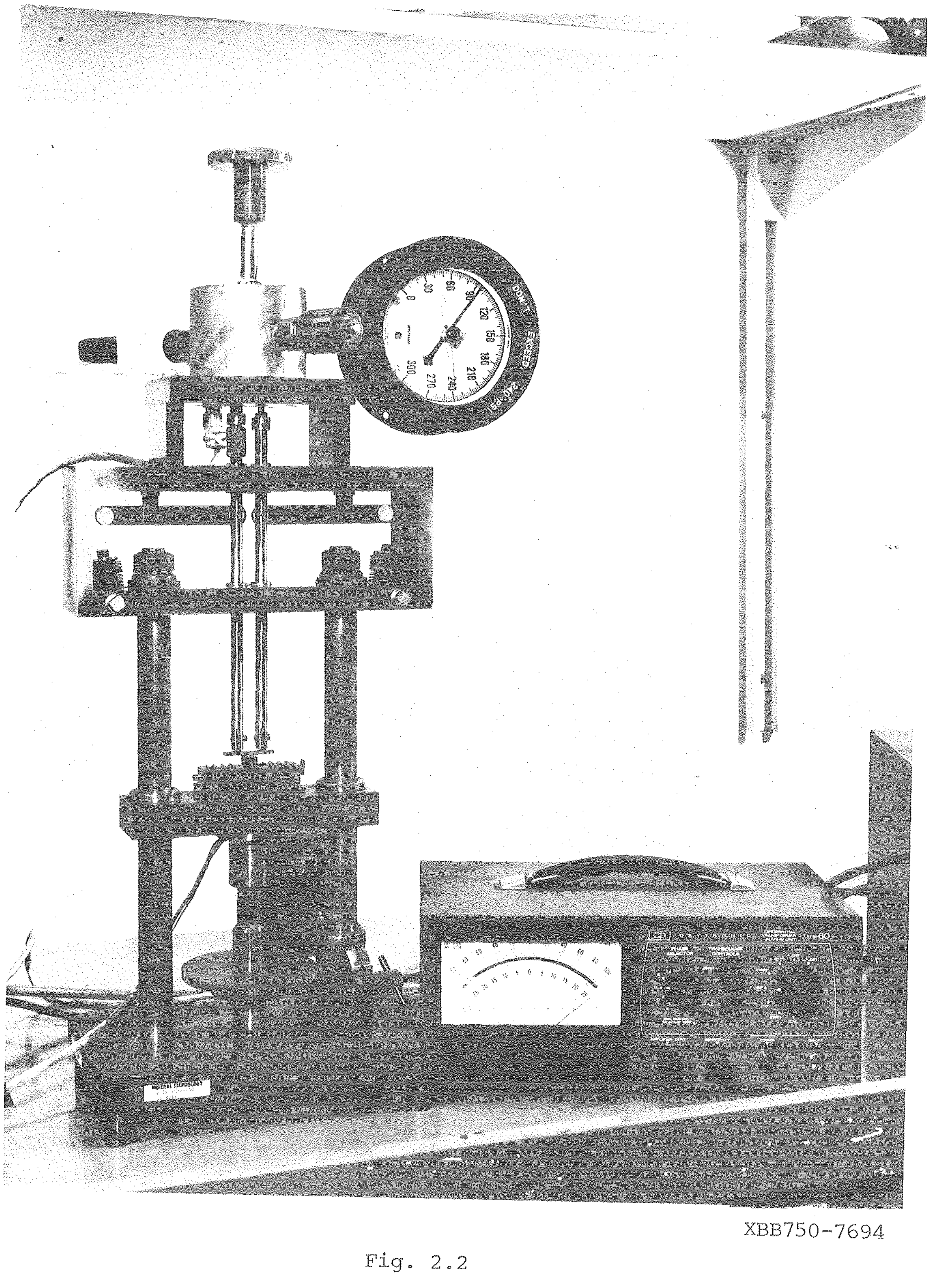

XBB750-7694

Fig. 2.2

3. DEVELOPMENT

It is intended that this section presents in some coherent manner several hypotheses which could explain the strength data generated in this study. Comparison of model predictions to actual data will be deferred until section four. However, brief discussion of the implications of each hypothesis will be presented with its development.

In order to place Weibull's general statistical approach, which is based on weakest link theory, into historical perspective, it is interesting to note that Weibull first published his theory in 1939, nineteen years after Griffith's paper and ten years after development of extreme value theory. For sake of comparison, standardized methods of valuating fracture toughness were not published until 1965.[11] Although the Weibull approach contains some fundamental limitations,[9] it has provided fit for data up to the present day.

Only with the recent need to develop structural materials with better reliability in high temperature and corrosive environments, such as gas turbines, nuclear reactors and coal gasifiers, has work on fracture statistics received more complete attention. Much of the recent work on fracture statistics is based on extreme value statistics with little regard to the microstructure of the material. However, recent work by McClintock[3] and others[9,12] develop fracture statistics from not only statistical theory but also with consideration of the microstructural parameters which can influence the physical properties. Efforts in correlating observed material flaws with strength measurements have been aided with recent tabulations of elasticity solutions of complex flaw geometries.[13,14]

In the development of this section Weibull's analysis is given the first and the most detailed treatment because of its widespread use and because the approach and methods used by Weibull are extended and used as a basis for the other hypotheses. After development of the Weibull approach possible extensions based on assumptions concerning the nature of the flaws are proposed; elasticity and linear elastic fracture mechanics (LEFM) solutions are utilized. These extensions of the Weibull approach are presented in general forms so that trends may be predicted. Prediction of absolute values of strength would require much further refinement.

The Weibull Analysis

The most universally used method of describing the variations in strength of "identical" specimens was pioneered by Weibull. He reasoned that since strength of a body is dependent upon the severity of the flaw causing failure, as was shown some years earlier by Griffith, and that since seemingly identical bodies show significant variations in strength, there must be flaws of varying severity within the body. By assuming that a single severe flaw propagates to final material failure without interacting with other flaws, he was able to utilize weakest link theory.

It can be shown by weakest link theory that the probability of survival, P_s of a body which fails from a single volumetric flaw is given by:

$$P_s = \exp[- \int_{vol} g(S)\, dV] \tag{3.1}$$

where g(S), the volumetric strength function, is a function of the density and severity distributions (size, shape and orientation) of flaws in the volume. Weibull chose a function of the form

$$g(S) = (S/S_o)^m \tag{3.2}$$

to describe the volumetric strength distribution and termed the integral over the volume the Risk of Rupture, B:

$$B = \int_{vol} g(S)\ dV = \int_{vol} (S/S_o)^m\ dV \tag{3.3}$$

The probability of survival can then be related to the stress on the sample (S), characteristic strength (S_o) and spread about the characteristic strength (m, the Weibull modulus). With this equation Weibull was not only able to accurately describe the spread of strengths about a characteristic value for "identical" specimens but could also predict reduction in median strength when specimens of increased volume were tested.

The calculation of the Risk of Rupture in specimens tested in four-point bending, Fig. 3.1a, is complicated by the fact that the stress in the specimen is not constant with position in the specimen (Figs. 3.1b, 3.1c). The combination of flaw severity and applied stress at the flaw determines whether the flaw will propagate. Assuming that only the flaws in the tensile regions of the specimen can cause failure, the Risk of Rupture in four-point bending may be written:

$$B = \frac{wh}{2(m+1)} \left(\ell_1 + \frac{\ell_2}{m+1}\right) \left(\frac{S_{TS}}{S_o}\right)^m \quad \text{(Derivation: Appendix 1)} \tag{3.4}$$

For a finite number of specimens, N, which are ranked in order of increasing strength, 1...j...N, the probability of survival can be approximated:

$$P_s = 1 - \frac{j - 0.3}{N + 0.4} \tag{3.5}$$

Substituting these expressions for B and P_s into equation (3.1) we obtain

$$1 - \frac{j - 0.3}{N + 0.4} = \exp\left(- \frac{wh}{2(m+1)}\right)\left(\ell_1 + \frac{\ell_2}{m+1}\right)\left(\frac{S_{TS}}{S_o}\right)^m \tag{3.6}$$

Taking the natural logarithm of both sides twice:

$$\ell n\ \ell n \left(\frac{1}{1 - \frac{j - 0.3}{N + 0.4}}\right) = m\ \ell n\ (S_{TS}) + \ell n\left[\left(\frac{wh}{2(m+1)}\right)\left(\ell 1 + \frac{\ell_2}{m+1}\right)\left(\ell_1 + \frac{\ell_2}{m+1}\right)\right] S_o^{-m} \tag{3.7}$$

Since this equation is of the form y = ax+b, when the experimental values of strength (S_{TS}) and rank (j) are plotted, the slope of the least squares fit of the data is the Weibull modulus, m. The characteristic strength can be computed from the relationship:

$$S_o = \left[\frac{-wh\left(\ell_1 + \frac{\ell_2}{m+1}\right)}{2(m+1)\ \ell n\left(1 - \frac{j - 0.3}{N + 0.4}\right)}\right]^{1/m} S_{TS} \tag{3.8}$$

For the median strength value, S_{med},

$$S_o = \left[\frac{wh\left(\ell_1 + \frac{\ell_2}{m+1}\right)}{1.386\ (m+1)}\right]^{1/m} S_{med} \tag{3.9}$$

The Weibull approach places restrictions on the homogeneity of the material. It is evident that, if there are flaws of varying severity randomly distributed within the volume, the material is not homogeneous on a microscale. However, in order to meet Weibull's criterion for homogeneity, the material must be homogeneous on a macroscale; the flaw severity distribution must be random within the material. This leads to an interesting contradiction of Weibull's assumption of no flaw-flaw interaction: if flaws are distributed randomly within the body, there is a finite probability of a flaw existing within the stress field of another flaw. Correcting for this stress field overlap in the Risk of Rupture calculation would be difficult because correction would require expressions for density, size distribution, shape distribution and orientation distribution of the flaws in addition to accurate elasticity solutions describing the stress fields. It must be assumed that interacting flaws are considered as one large flaw.

Introduced Stress Fields

When large numbers of mechanical discontinuities are introduced into the material, modifications must be made to the Risk of Rupture calculation in the Weibull approach because mechanical discontinuities change the stress distribution in the surrounding material.

Vardar et al.[1] considered the state of stress around a spherical void, as derived by Goodier,[2] and corrected the Risk of Rupture calculation for the superimposed stress distribution. Their approach also took into account an increase in the nominal stress due to reduction of cross-sectional area of the matrix. The Vardar approach assumes that the material is homogeneous and that the introduced voids do not change the failure mechanism or the intrinsic flaws; a reduction in strength is due only to the increased stress level in the small volume near the voids. It must be emphasized, however, that, due to the statistical nature of flaw size and spatial distribution, the flaw causing failure need not be within the stress field of a void. For this reason the Risk of Rupture calculation also includes a term for the volume of material which sees only the nominal stress. Also, Vardar estimates that complications arising from void stress field overlap, limit his analysis to a void fraction of approximately 0.10.

Due to the complexity of the calculations, only the results are quoted here:

$$B = \left(\frac{S_{TS}}{S_{TS}(o)}\right)^{m} V \quad (1+V_v)^{-m} \quad (1-V_v{}^{3}) + \frac{3(2m+1)}{2^{\;2}} \; V_v \; H(m) \qquad (3.10)$$

H(m) and depend upon the choice of limits over which the stress field of the spherical void is integrated. Because an analytic solution was not possible, the numerical results for the median strength (P_s = 0.5 or B = 0.693) are presented in graphical form for ν = 0.20 (Fig. 3.2).

Several interesting conclusions can be drawn from Vardar's analysis. First, voids are not the cause of failure, per se, but rather it is the stress field of these voids which interacts with intrinsic flaws causing the intrinsic flaws to propagate to final failure. Second, the reduction in strength is a function of the volume fraction of voids but is independent of void size. Finally, since the flaw population does not change with the introduction of voids, it is expected that the derivative of the plot of failure stress would be continuous to zero volume fraction of voids; i.e., the fracture stress should not drop discontinuously with the introduction of the first void.

Void-Grain Boundary Interactions

A possible modification of the Weibull analysis is to assume the nature of the flaws causing failure or, more precisely, whether the flaws which cause final failure are associated with any specific microstructural feature. Weibull assumed that flaws were a volume effect and did not directly speculate on their nature. This approach, while useful, would be more informative if it would indicate something about the flaw itself, either in a positive or negative sense, so that "materials engineering" could be performed. That is, if flaws are associated with, say, grain boundaries, then a compromise of the number of grain boundaries (statistical nature of flaw size) and the length of grain boundaries (size of flaws) might be attempted. As another example, Vardar's analysis, if correct, indicates that if we model the pores in a ceramic system as spherical voids, then the strength distribution and median strength are dependent on volume fraction of porosity and not on pore size. From a practical standpoint, processing might then be adjusted so that pores which are detectable by standard nondestrictive examination techniques are produced.

When associating flaws with microstructural features a logical starting point is to assume that flaws are associated with grain boundaries. As a precedent McClintock[3] assumed that cracks are random aggregations of unbonded grain boundaries. Although the condition that grain boundaries are unbonded may be a bit extreme, the large fraction of intergranular fracture in many ceramic materials indicates that grain boundaries tend to be weaker than the grains themselves.

The first approach could be an extension of Vardar's analysis by assuming that the Risk of Rupture is proportional to the number of grain boundaries within the stress field of the void, much as Weibull assumes that the Risk of Rupture is proportional to the volume of stressed material. This would result in equations similar to Vardar's (Eq. 3.9) with a grain size term. For specimens with equal grain size the resulting equation would be identical to Vardar's equation in form and in the prediction that there would be no void size dependence.

Another assumption that could be made is that the Risk of Rupture is proportional to the number of grain boundaries intersecting the void surface. The number of grain boundary-void intersections, N_{GB}, can be written:

$$N_{GB} = \int_{\text{voids}} \frac{d^2}{G^2} = \int_V N_v \frac{d^2}{G^2} \, dV \tag{3.11}$$

Substituting for N_v and integrating we obtain:

$$N_{GB} = V \frac{6V_v}{dG^2} \tag{3.12}$$

Physically, Weibull associated flaws with the volume of the specimen. When associating flaws with a specific microstructural feature, ie, the grain boundary-void intersections, we replace the volume in the Weibull expression by the number of these features in the sample:

$$B = \frac{3V_v \, Vwh}{dG^2(m+1)} \left(1 + \frac{2}{m+1}\right) \left(\ell_1 + \frac{2}{m+1}\right) \left(\frac{S_{TS}}{S_o}\right)^m \tag{3.13}$$

Solving for the median strength we obtain:

$$S_{med} = \frac{V_v \, wh}{dG^2(m+1)} \left(1 + \frac{\ell_2}{m+1}\right) \left(\ell_1 + \frac{2}{m+1}\right)^{-1/m} S_o \tag{3.14}$$

We must digress here to consider the physical meaning of the characteristic strength. Weibull in his formulation of the Risk of Rupture did not attach a direct meaning to the characteristic strength other than that as a scale factor for the strengths of different materials. However, when we use the Weibull formulation to predict the strength of specimens of varying volumes or specimens under varying loading conditions (three point bending, four point bending, uniaxial tension) we have assumed that the characteristic strength is a property of the material. In addition, Vardar's derivation assumes that the material fails from inherent flaws; therefore the characteristic strength must be a material property independent of the void diameter and volume fraction. Because similar arguments may be used with the Weibull Modulus we shall also consider m a material property, thus constant.

Returning to our previous reasoning, if we assume G, S_o and m constant in all specimens, then:

$$S_{med} = C\left[\frac{d}{V_v}\right]^{1/m} \tag{3.15}$$

and

$$\ell n\ S_{med} = \frac{1}{m}\ \ell n\ \left(\frac{d}{V_v}\right) + C \tag{3.16}$$

When $\ell n\ S_{med}$ is plotted against $\ell n(d/V_v)$ for each of the void size/void volume fraction sets then a straight line should result with a slope of $\frac{1}{m}$, if the failure occurs at the "weakest" grain boundary-void intersection.

We can make two predictions from this hypothesis. First, the median strength should decrease as the volume fraction of voids increases. Second, for equal volume fractions of voids the large voids should be less detrimental to strength than the small voids.

Note, it would not be expected that this model would be valid when a poor statistical sampling of grain boundary-void intersections occurs ($V_v \to 0$) or when void-void interactions occur ($V_v \geqslant 0.10$).

<u>Voids as Flaws</u>

Linear elastic fracture mechanics (LEFM) has been used to predict flaw size at fracture from the strength data and fracture toughness values. However, due to the difficulty of producing accurate flaw sizes and tip sharpness and the difficulty in measuring these quantities, the prediction of strength from measured flaws is performed infrequently.

For blunt mechanical discontinuities, such as spherical voids, LEFM solutions are not expected to apply as sharp crack tips are necessary. However, in a polycrystalline specimen with many grains on the surface of the void, grain boundary grooving is expected to occur due to the differences in surface energy of the grain-grain interface and the grain-vapor interface. Thermodynamics predicts that the groove is sharp to atomic dimensions, therefore, LEFM is expected to apply to even the "blunt" spherical voids if the voids have several grain boundaries exposed on the surface during sintering. Note that flawed or cracked grain boundaries, as required by McClintock, are not necessary.

If the gross assumption is made that the 2-dimensional LEFM solution for the penny-shaped flaw approximates the 3-dimensional case of the spherical void, then:

$$\sigma_f = K_{IC} \; (Yd)^{-1/2} = Cd^{-1/2} \qquad (3.17)$$

Variations in fracture strength then must be related to the variation in the void sizes and the probability of finding a large void in a region of high nominal stress.

When the void densities (statistical sampling) and volumes of specimens are equal, then the median fracture strengths of groups of samples should be related by:

$$\frac{S_{med\ 1}}{S_{med\ 2}} = \left(\frac{d_2}{d_1}\right)^{1/2} \qquad (3.18)$$

when

$$N_{v_1} = N_{v_2}$$

or:

$$\left(\frac{V_{v_1}}{V_{v_2}}\right)^{1/3} = \frac{d_1}{d_2} \tag{3.19}$$

Substituting equation (3.19) into equation (3.13) we obtain:

$$\frac{S_{med\ 1}}{S_{med\ 2}} = \left(\frac{V_{v_2}}{V_{v_1}}\right)^{1/6} \tag{3.20}$$

In addition, the ratio of the strongest to weakest specimens in a group would necessarily be less than or equal to the square root of the ratio of the smallest to largest void sizes:

$$\frac{S_{TS\ max}}{S_{TS\ min}} \leqslant \left(\frac{d_{min}}{d_{max}}\right)^{1/2} \tag{3.21}$$

This hypothesis predicts a definite strength dependence on the void diameter but predicts very slight influence of changes in void fraction.

Flaw-Flaw Interaction

As first noted by Weibull, statistical strength theories place restrictions on the homogeneity of the material; flaw-flaw interactions are assumed to not occur. Due to the statistical nature of flaw size, shape, orientation and distribution and the complexity of stress distribution around complex flaw shapes there is little hope of accurately predicting the effect of flaw-flaw interaction on the strength of brittle solids.

Perhaps the simplest case of flaw-flaw interaction is one of spherical voids randomly distributed in a matrix. For this case the stress distribution around isolated voids is known, as are, obviously, size, shape and spatial distribution of voids. If the voids are distributed randomly, we would expect clustering of voids thus changes in the stress field. Now, even in this least difficult solution we must determine the following:

1. Probabilities of 1,2,3,...,n voids clustering
2. Probability of shapes occurring, ie, void-void orientations
3. Probability of cluster orientations
4. Stress fields around clusters of 1,2,3,...,n voids.

Since each of these four calculations is formidable and beyond the scope of this work, a more general approach will be taken.

It can be shown that the probability of a cluster of n voids depends on the void density (number per unit volume, N_v) and that equal void densities have equal probabilities for a cluster of n voids. Equal void densities occur when the relation

$$\left(\frac{V_{v_1}}{V_{v_2}}\right)^{1/3} = \frac{d_1}{d_2} \qquad (3.19)$$

is satisfied. Furthermore, the physical dimension which describes the flaw size, a, is proportional to the diameter of the voids occurring in the cluster. From LEFM the fracture stress can then be given:

$$\sigma_f = K_{IC} \, (Y_a)^{-1/2} = C(d)^{-1/2} \qquad (3.17)$$

where Y is a flaw shape and orientation factor. If we compare median strengths and combine equations (3.19) and (3.17), we obtain:

$$\frac{S_{med_1}}{S_{med_2}} = \left(\frac{V_{v_2}}{V_{v_1}}\right)^{1/6} \tag{3.20}$$

Note that this is the same relationship as obtained when discussing voids as flaws.

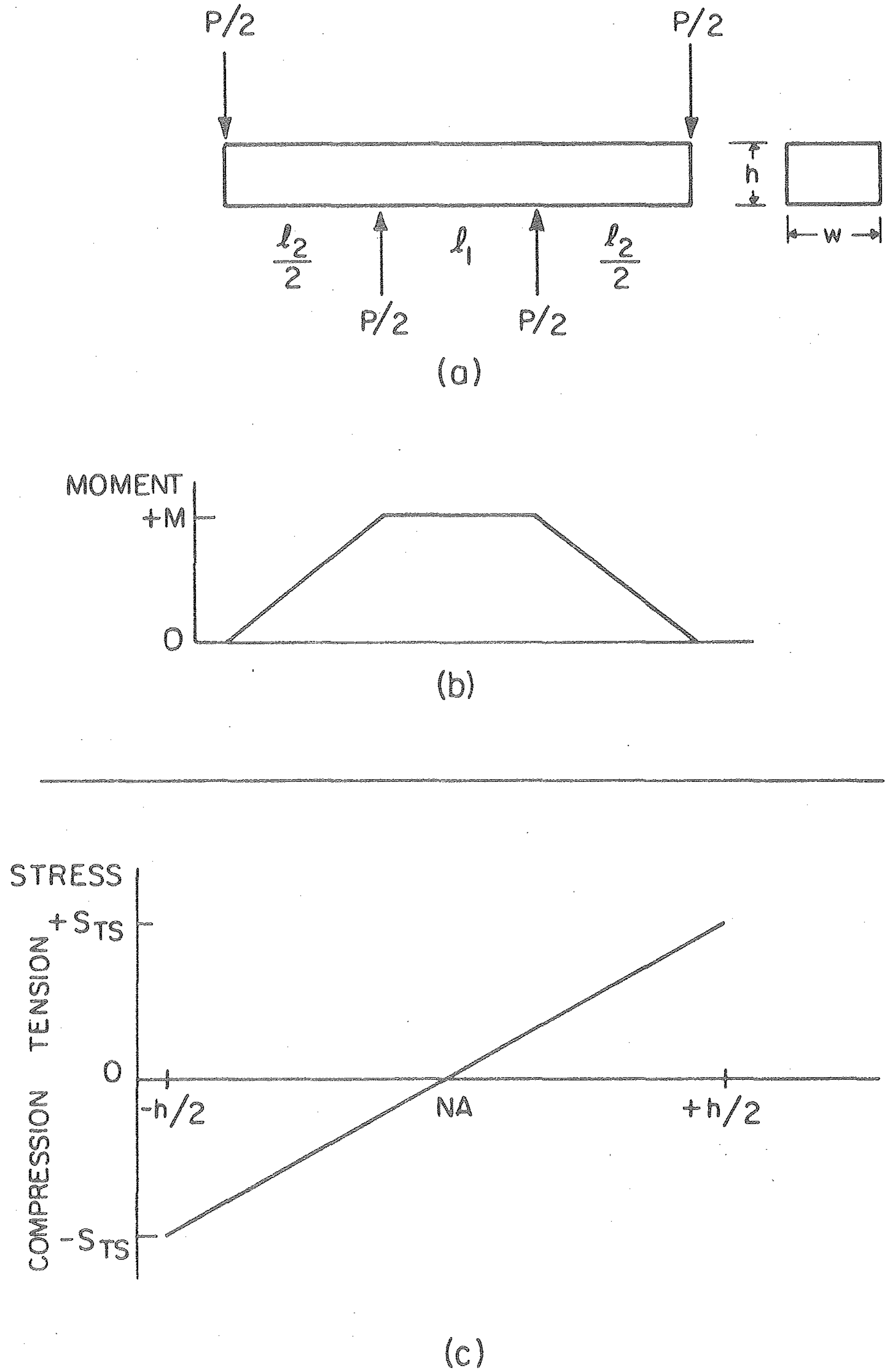

XBL789-5755

Fig. 3.1

(a) Loading of test specimen.

(b) Moment distribution, longitudinal direction.

(c) Stress distribution, thickness direction.

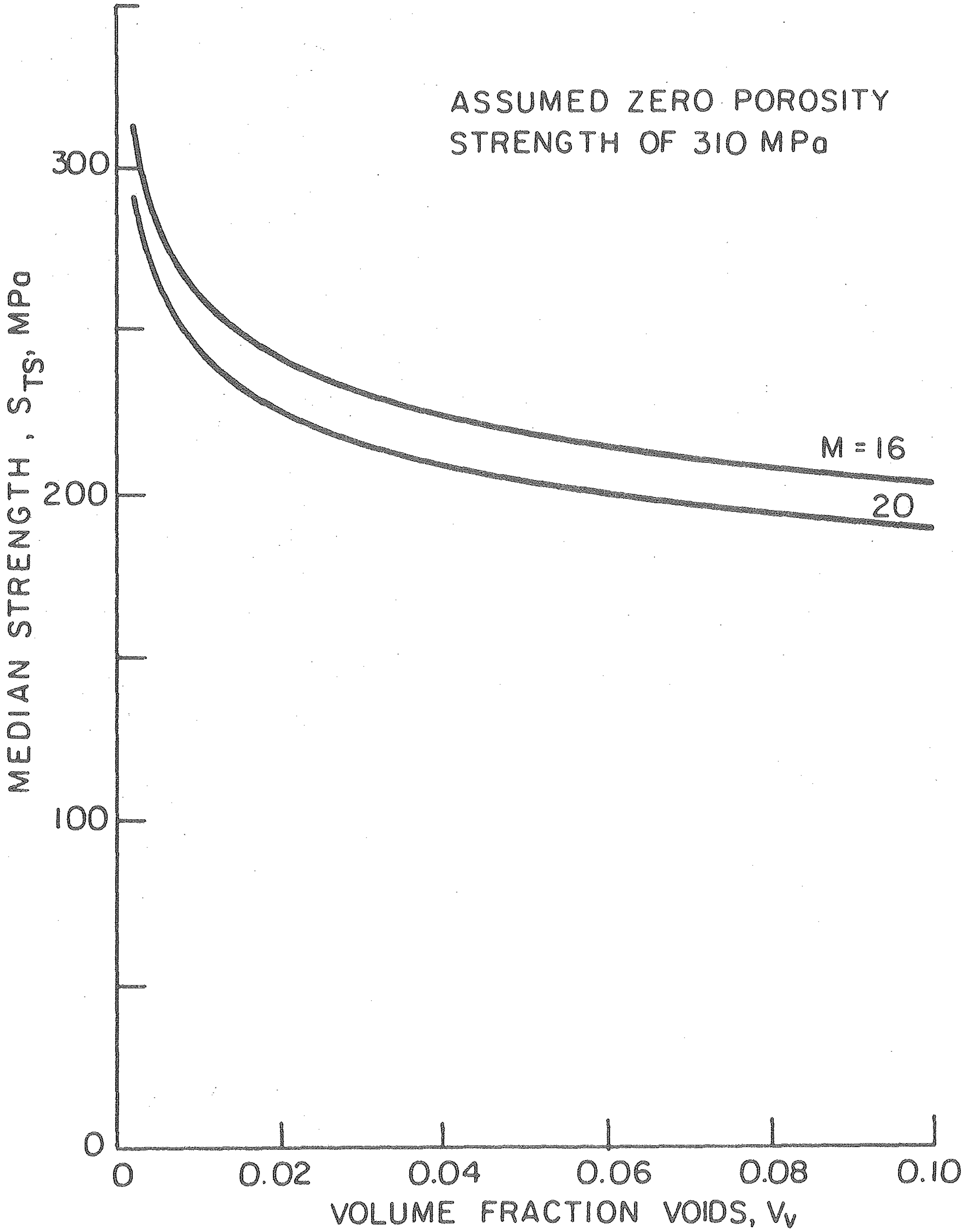

XBL 789-5756

Fig. 3.2

4. RESULTS AND DISCUSSION

Microstructure

The understanding of virtually all phenomona which involve materials necessarily includes evaluation of the microstructure for possible effects. This microstructural evaluation should take place prior to evaluation of other data in order that experimental variables are better understood and better utilized.

Preliminary work on the selection of the organic used in the generation of voids indicated that a residue of 0.025% of the organic remained after calcination. It has been well documented[25] that trace impurities can concentrate at grain boundaries and affect the grain boundary surface energy and thus the sintering behavior and, if the fracture path occurs along grain boundaries (intergranular), the strength. In order to determine if the trace impurities from the organic had a significant effect it was necessary to analyze the microstructure for changes with changing impurity content. Changes in grain boundary energy would necessarily change the driving force for sintering and grain growth. This in turn would result in variations in grain size.

Lineal analysis of random microstructures yielded a mean grain size of 8.8 μm with no significant size variations with changes in amount of organic added. Analysis of the small regions near voids yielded a grain size similar to that away from voids and in the dense specimens (Fig. 4.1 - 4.3).

Fractographic analysis, which will be discussed later, revealed no definite differences in the fraction of intergranular fracture occurring in dense specimens and in specimens with voids, indicating that the grain boundaries in the specimens with voids are not significantly stronger or weaker than those in the dense specimens. Because no changes occurred in grain sizes or fracture surfaces it is concluded that any residue from the organic had no effect on the measured properties of the specimens.

The distribution of extrinsic voids is clearly shown in Figs. 4.4-4.6. Note that even though there are clusters of voids evident in the surface, relatively few voids are touching. This would indicate that the clustering is not due to some attractive force such as electrostatic attraction but, rather, is due to random fluctuations in void distribution. A random cut through the matrix clearly indicates that the extrinsic voids are spherical in shape and exist in a dense matrix (Fig. 4.3).

Typical tensile surfaces are shown in Figs. 4.7-4.9. In particular, note that the surfaces are in the as-cut condition, as indicated by the scratches (Fig. 4.7), and that the scratches are nearly perpendicular to the fracture plane. Higher magnification of the tensile surface reveals few pullouts and a limited amount of transgranular fracture. Examination of the void edges (Fig. 4.7) indicates that some chipping occurs during cutting. It is interesting to note in Fig. 4.7 that the fracture does not proceed through the cluster of six voids on the tensile surface. This would seem to indicate that the stress field from single voids and clusters of voids decays rapidly and that there is little interaction between the propagating crack and other "flaws" in the material.

The choice of a "typical" fracture surface is a difficult task because localized regions are often predominantly intergranular (Fig. 4.10) or transgranular (Fig. 4.11). Stereological evaluation of several representative random fracture surfaces indicates that 60% of the cross-section fractured in an intergranular mode with the remaining 40% in a transgranular mode. A representative fracture surface (~65% intergranular fracture) is shown in Fig. 4.12. No statistically valid differences in the fraction of intergranular fracture could be detected between those specimens which contain voids and those which did not.

Rice[18] noted that in many materials in which the primary fracture mode is intergranular there is a change to transgranular fracture around naturally occurring pores. In material with artificially produced voids there also seems to be a similar change as the crack front propagates past single voids or clusters of voids (Figs. 4.11, 4.13 and 4.18). It is believed that this behavior is due to a change in the state of stress at the crack tip because the fracture mode changes when the crack front passes the voids rather than as it approaches them. It must be noted that the change in fracture mode does not always occur when the crack front passes a void (Fig. 4.10).

If the regions of transgranular fracture are examined closely it becomes apparent that there are two modes of transgranular fracture:

1, Fracture which is independent of crystallographic direction as indicated by smooth curved surfaces (Fig. 4.11) and 2, Fracture which follows crystallographic directions (cleavage) as indicated by steps and notched surfaces on a single grain (Fig. 4.15). Very little of the transgranular fracture occurs along crystallographic planes (the second mode). Although the regions which fracture in the first transgranular mode are relatively featureless, thermal etching of the grain boundaries (Fig. 4.14) reveals that this transgranular region actually encompasses many grains; the transgranular fracture is not due to a single large grain and does not revert to intergranular fracture at the first grain boundary but, on the average, propagates through several grains.

It may be appropriate here to reiterate that the primary fracture mode in all samples (with or without voids) is intergranular and that voids are not necessary for transgranular fracture to occur (Fig. 4.15).

Strength Data and Calculated Values

After reducing the raw data to the calculated values presented in Table I, the first task was to compare these data with proposed empirical and phenomonological strength-porosity relationships. (see reference 20 for a summary) Most of these proposed relationships considered only total pore volume and did not consider the effects of pore size and shape. The data from this study (Fig. 4.19) indicate that there is a definite void size effect; therefore, these proposed relationships could be discarded immediately. Unfortunately, the remaining relationships which predicted a pore size dependence were not able to accurately predict the data. Only the Weibull approach and extensions of the Weibull approach remained as possible "explanations" of the data.

Presented in Table I are the values calculated from the raw data. Both mean and median strength values are reported. The consistency in the experimental values is reflected in the small coefficient of variation values.

A few comments about the calculated strength values are appropriate here. First, all reported values of the strength (S_{TS}) will refer to the median strength values, unless otherwise noted, ie, the Characteristic Strength (S_o). Second, as shown in the curves (Fig. 4.19) and the data (Table I), the strength-void fraction relationships are very consistent and reproducible within the void fraction range studied. Also, as shown in Fig. 4.20, there is a definite relationship between the median and Characteristic strengths. It is expected that this relationship, as well as the extrapolation, is accurate since the least squares fit of the data extrapolates through the origin.

The Weibull Analysis

The values of the Weibull parameters, S_o and m, reported in Table I are calculated from a least squares fit of individual sets of data by methods described in section 3. The weighted mean of the individual m values is 20.6. Since variations in m values cannot be correlated with variations in void densities, it is believed that the scatter in individual m values is due to the small number of specimens being tested. It can easily be seen that one or two high or low strength values out of ten can significantly affect the slope of the P_s-S_{TS} curve but have relatively little effect on the median value. This viewpoint is further strengthened by noting that there is a definite relationship between the coefficient of variation of the strength, CV, and m (Fig. 4.21). When a weighted mean of the CV values is used in conjunction with the experimentally derived CV-m curve, a m value of 20.6 is predicted. This prediction compares favorably with that of the weighted mean of the m values (20.6) and, as discussed later, the m value of all normalized data (21.7). For sake of comparison a proposed relationship[21]

$$CV = \left(\frac{1}{m}\right)^{0.94} \tag{4.4}$$

is also presented. Even though the experimental points do not lie on the proposed curve, the consistency of the data and the parallel nature of the two curves is obvious.

Finnie[21] indicated that data from different sizes of specimens and different types of tests can be pooled if each strength observation is normalized by the median strength for that set of specimens. When the strength values of the specimens of a set (void fraction-void size) were normalized by the median strength of that set and the normalized values for all 198 bend specimens were ranked and plotted, the composite curve in Fig. 4.22 resulted. A least squares fit of these data yielded an m value (slope) of 21.7, a value nearly equal to that of the weighted mean of the m values (20.6). Close examination of the curve indicates separate regions of different slopes. The change in slope, if significant, could indicate the existance of two separate flaw populations. Since previous work[17] indicated that surface flaws were not one of the populations, both populations would necessarily exist within the bulk of the material.

We must digress here to further consider the meaning of Characteristic Strength and the relationship to the material under consideration. As discussed in section 3, the prediction of strength for specimens of volume differing from that of the test volume assumes that the Characteristic Strengths and Weibull Moduli are identical for each sample of material. This assumption states that the failure mechanisms and flaw populations are the same for each sample; for a given loading condition (state of stress) the Weibull parameters must be constants characterizing the particular batch of materials. Conversely, for similar loading conditions (state of stress) and failure mechanisms (flaw populations) the Weibull parameters must be identical for each set of specimens independent of stressed volume. It must be noted, as discussed by Pankow,[19] that Weibull parameters are not constant when the stressed volume becomes extremely small. The reason for this is presumably due to changes in the failure mechanism or inhomogeneity on a microscale. This of course places limits on the minimum size of the stressed volumes if valid comparisons of Weibull parameters are to be made.

In order to compare the stressed volumes of samples which contain introduced discontinuities it is not sufficient to compare bulk volumes.

Instead, we must calculate the volume of material which sees the stress field of the discontinuity superimposed over the nominal stress field; for convenience we shall call this volume the stressed volume. It can be shown that the stressed volume of samples which contain voids is dependent only on the void fraction (independent of void size). Assuming that the specimen fails from a flaw within the stressed volume (rather than from a flaw within the nominal stress field) then a plot of S_o-V_v should yield a single curve for all void sizes. It can be seen in Fig. 4.23 that all data does not fall on a single curve (correlation coefficient for a straight line is 0.87). Closer examination of the data points indicates that there are three independent curves, each representing a different void size (Fig. 4.24). Least squares fit of the data points indicates an excellent straight line fit for the 48 μm and 80 μm voids (correlation coefficient $\geqslant$ 0.96); it becomes obvious that the data points are members of distinct families. The data for the 28 μm voids is not so convincing. The reason for the greater scatter for the S_o values of the 28 μm void size is not obvious at this time.

The fact that distinct curves exist for different void diameter indicates that fundamental errors exist in this formulation. One of the more satisfying explanations is that the stress field of a void does not extend over several grain boundaries for the smaller void sizes. This is not a problem in statistical sampling of single grain boundaries but, rather, a problem of sampling multiple continuous grain boundaries. This might also explain the scatter in the S_o values for the 28 μm void size. Another possible explanation is that the specimens do not fail from flaws within the stressed volume but from flaws within the nominal stress field. This change should result in very low m values for small void fractions because a few specimens would fail from flaws in the stress field of the void thus be very weak. However, the correlation between small V_v and small m does not seem to exist (Table I). Existence of varying values for S_o with changes in void fraction for the largest void size (80 μm) seems to indicate that statistical sampling errors may not be the cause of the variations but, rather, fundamental errors in this analysis and, perhaps, in the Weibull formulation may be the cause.

Introduced Stress Fields

Section 3 presented the Weibull approach and several modifications to the Weibull approach which might prove useful in analysis of the system under study. The work of Vardar et al[I] proposed to provide the most direct test of Weibull Statistics as no modifications were made to Weibull's analysis. Instead, modifications were made to the equations describing the stress field which existed within the sample, thus the Risk of Rupture.

The data presented in Vardar's paper supports his evaluation very well. However, the data generated in this study does not support the analysis nearly so well. Perhaps the most critical difference is the strength dependence on void size noted in this study. The Vardar modification of Weibull's analysis predicts that the strength of bodies which contain spherical voids is dependent on the void fraction and independent of void size. The data from this study indicates that the strength is a function of void size as well as void fraction and that the plots of $S_{med} - V_v$ are nearly linear over the void fraction ranges studied as opposed to his prediction. In addition, the median strengths at high void fractions are lower than predicted (Fig. 4.25).

The question becomes: What are the primary differences in the two studies? The fundamental difference seems to be in the choice of materials: lead-zirconate-titinate (PZT) versus alumina. A previous study[22] indicated that there is probably a continuous second phase present at grain boundaries in PZT due to the evaporative liquid-phase sintering technique used in material fabrication. Because PZT fails by a primarily intergranular mode, a grain boundary phase could have a significant influence on the strength. The alumina used in this study has no detectable second phase. A second difference is the grain size/void size ratio. It has been suggested[23] that the relatively small grain size/void size ratio in this study could account for the descrepancies. Indeed, it may be noted that the grain size/void size ratio for the largest void size (80 μm) is within the range studied by Vardar and provides the closest fit to his prediction for $0.02 < V_v < 0.06$. However, a significant deviation exists for $V_v > 0.07$.

Pankow[19] has indicated that for fracture statistics to be valid there should be greater than 100 stressed grain boundaries, perhaps several hundred. Examination of Fig. 4.5 seems to indicate that this criterion has been fulfilled, at least for the specimens with higher void fractions. If the statistical criterion has not been fulfilled then one would expect a rash of specimens which are stronger than predicted and thus a decrease in the slope of the Weibull plot. In fact, the Weibull plot of the normalized values (Fig. 4.22) does show a decrease in slope (if significant) but there appear to be far too many specimens in this region to correspond to only the small void fraction specimens.

<u>Extension of the Weibull Analysis Based on Microstructural Parameters</u>

Comparison of the data and the three hypothesis based on observable microstructural features, ie, void-grain boundary interaction, voids as flaw and flaw-flaw interactions, are lumped into this sub section for one reason: they do not correlate well with the data. Does this mean that there is no correlation between these microstructural features and strength? Based on the volume of evidence that observable micro-structural features and strength? Based on the volume of evidence that observable microstructural parameters have an effect on strength, ie, strength-grain size relationships, and relationships between changes in fracture mode and grain size, the answer to this question must be "NO".

Before proceeding further we should compare the experimental results to the predictions of these hypotheses. The void-grain boundary interaction hypothesis predicts that a plot of $\ln S_{med}$ vs. $\ln \left(\frac{d}{V_r}\right)$ will produce a single straight line for all void sizes with a slope of $\frac{1}{m}$. Plotting the data in this manner (Fig. 4.26) results in three separate curved lines. The voids as flaws and flaw-flaw interaction hypotheses both predict that a plot of S_{TS_1}/S_{TS_2} vs $(V_{v_2}/V_{v_1})^{1/6}$

will produce a straight line for all data points. Figure 4.27 indicates that three separate curves result (the curves are sketched in for clarification). Note that the relative values of S_{TS} and V_v are referenced to $S_{TS_2} = 235$ and $V_{v_2} = .038$ for the 48 μm void size. Even though this selection was arbitrary, other selections yielded similar results.

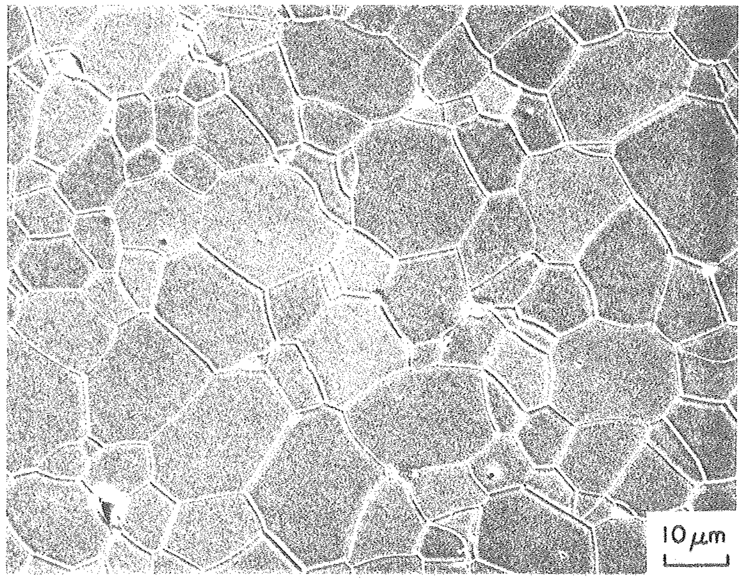

Fig. 4.1. Polished and thermally etched section of a dense specimen. $\bar{\ell}$ = 9.0

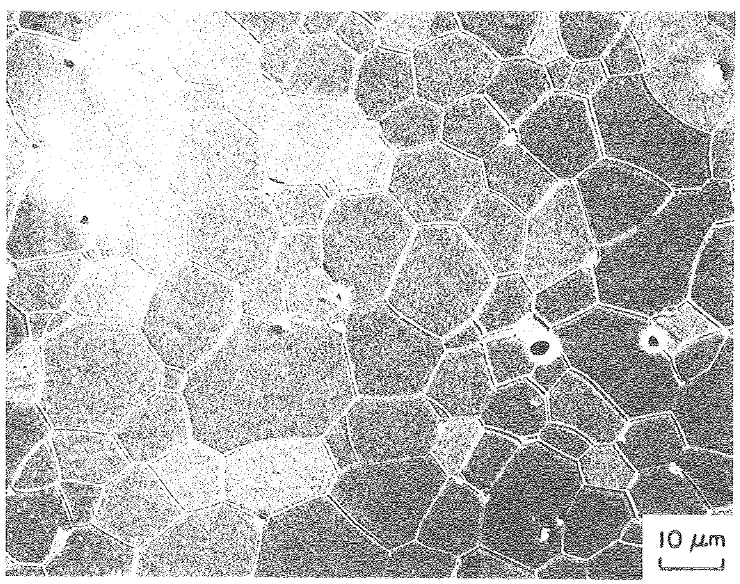

Fig. 4.2. Polished and eteched section of a specimen which contains 0.12 void fraction (voids not visable) $\bar{\ell}$ = 8.8 μm

XBB 789-10742

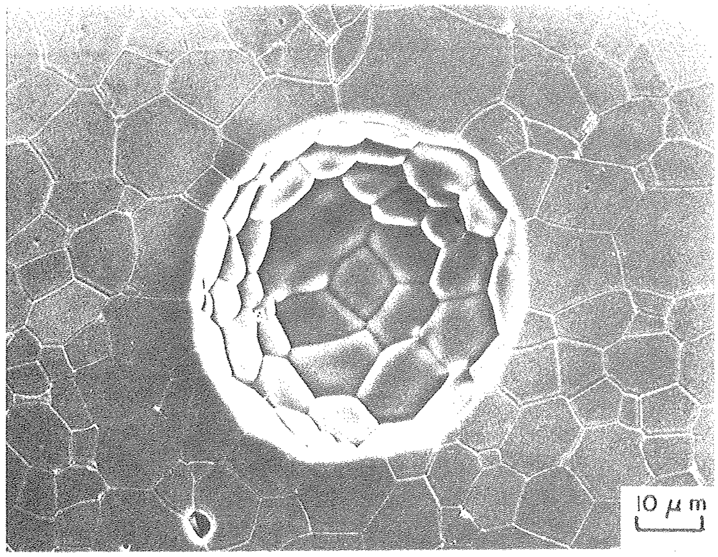

Fig. 4.3. Polished and etched section. Note the symmetry of the void and the large number of grain boundaries which intersect it.

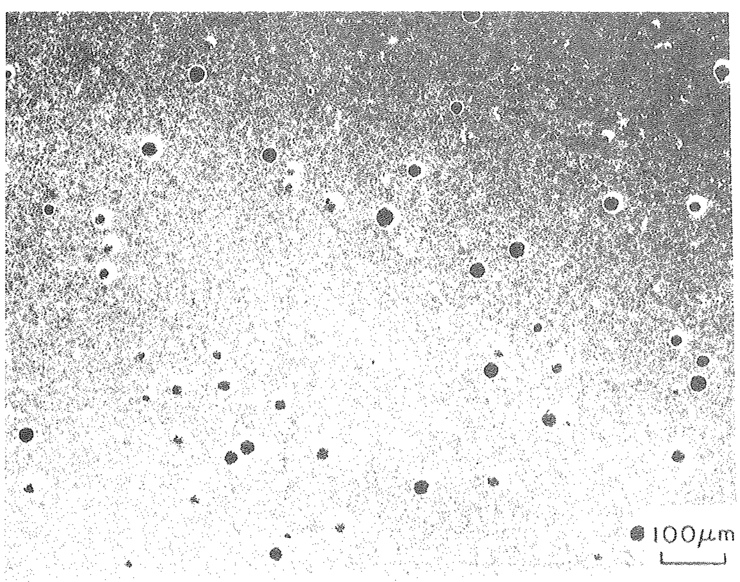

Fig. 4.4. Polished and etched section. ($V_v \sim 0.02$, $d = 28\ \mu m$)

XBB 789-10887

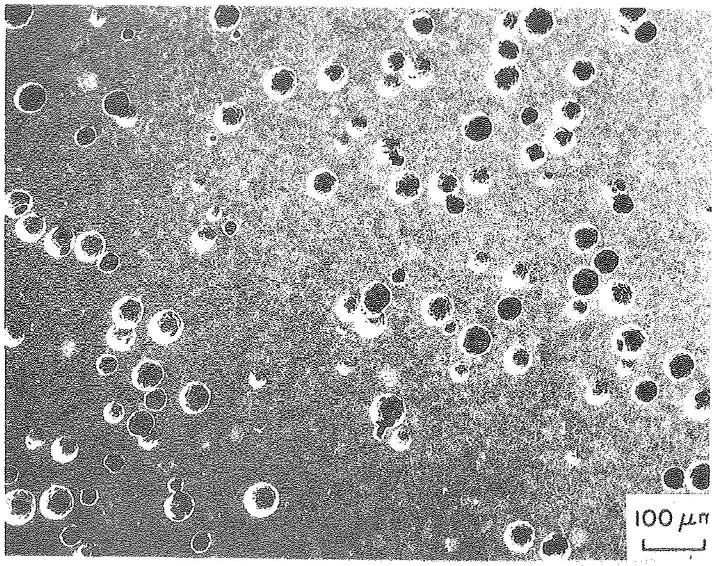

Fig. 4.5. Polished and etched section. ($V_v \sim 0.06$, $d = 48\,\mu m$) void clustering apparent.

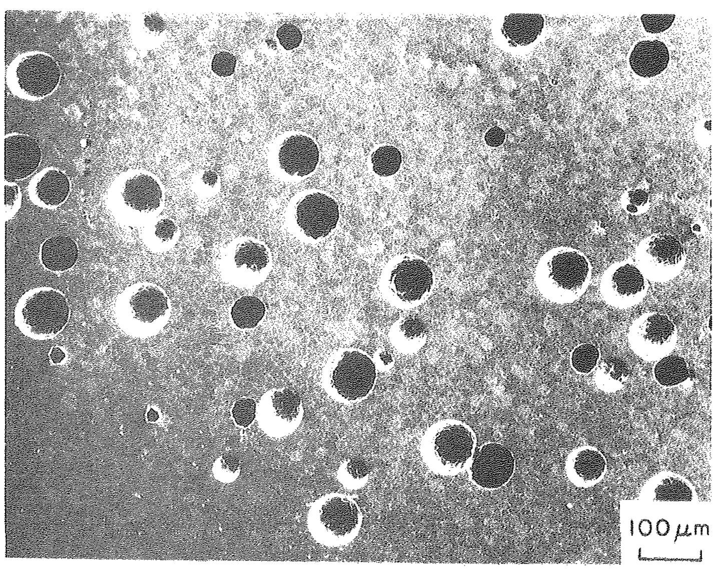

Fig. 4.6. Polished and etched section. ($V_v \sim 0.04$, $d = 80$) many voids approach each other but few actually touch.

XBB 789-10886

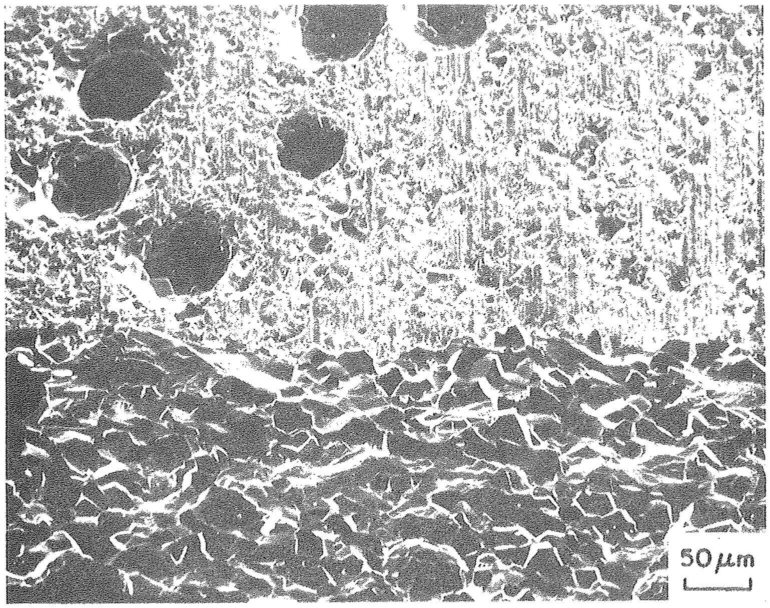

Fig. 4.7. As-cut tensile surface/fracture surface. The parallel lines are machining marks on the tensile surface.

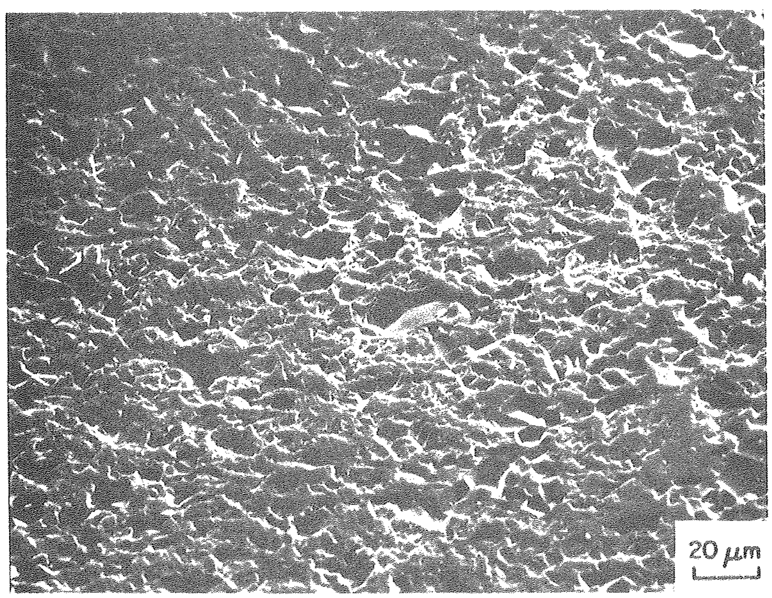

Fig. 4.8. As-cut tensile surface.

XBB 789-10747

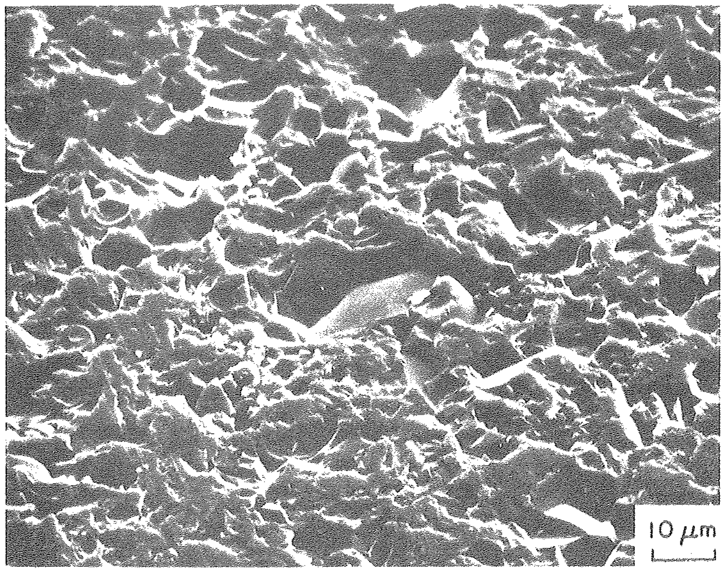

Fig. 4.9. Detail of as-cut tensile surface.

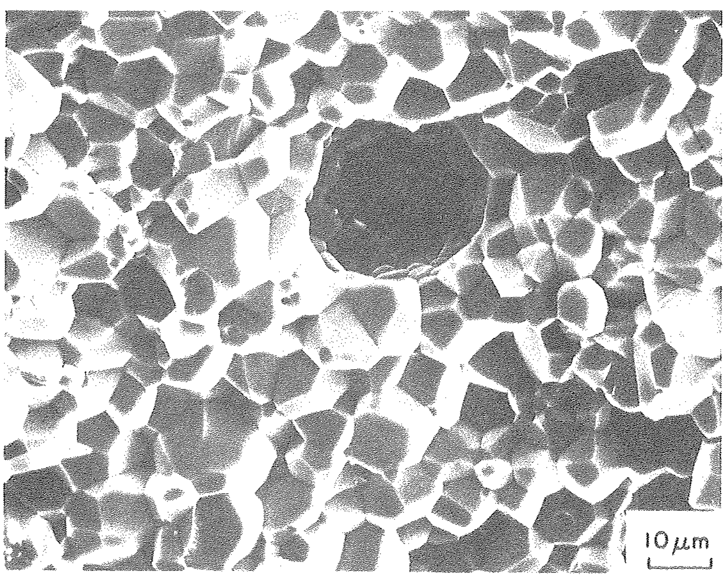

XBB 789-10746

Fig. 4.10. Fracture surface. Intergranular fracture near artificially produced void.

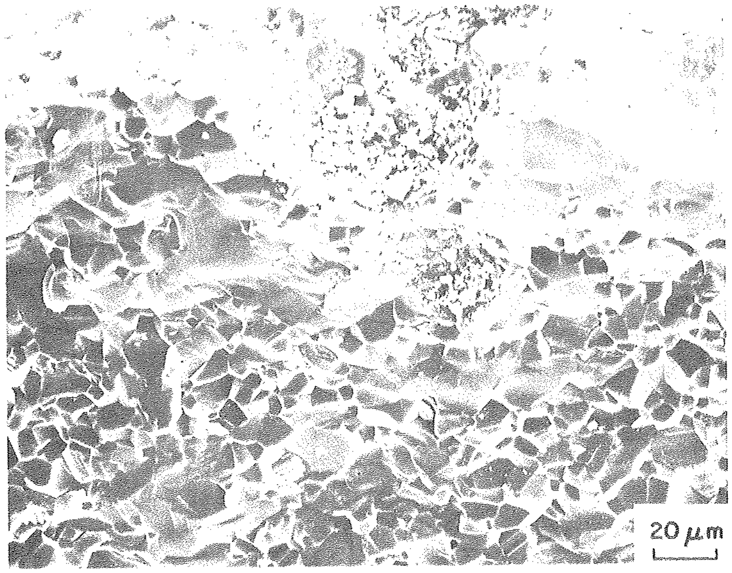

Fig. 4.11. Tensile surface/fracture surface. Predominantly transgranular fracture below tensile surface near voids.

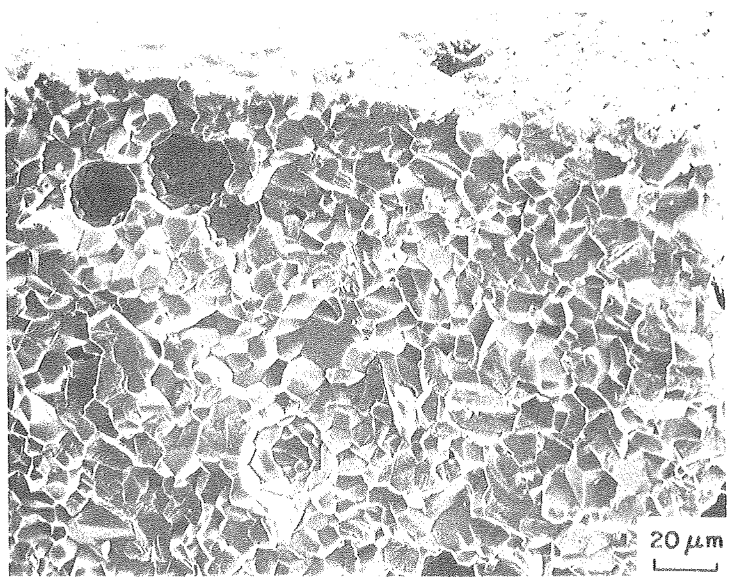

Fig. 4.12. Fracture surface/tensile surface. Predominantly intergranular fracture below tensile surface near voids.

XBB 789-10745

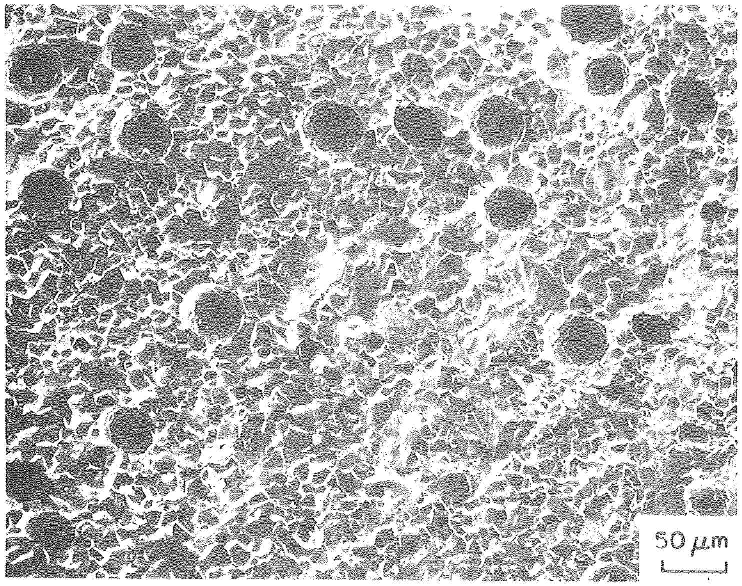

Fig. 4.13. Fracture surface. The direction of crack propagation is from top to bottom. Note the change in fracture mode when the crack passed the voids.

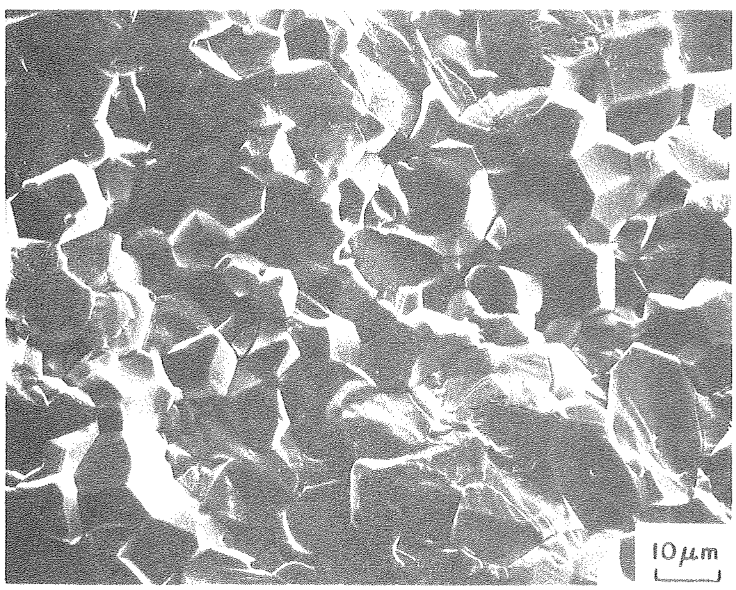

Fig. 4.14. Thermally etched fracture surface. The thermal etch delineates the grain boundaries in the otherwise featureless transgranular fracture region.

XBB 789-10741

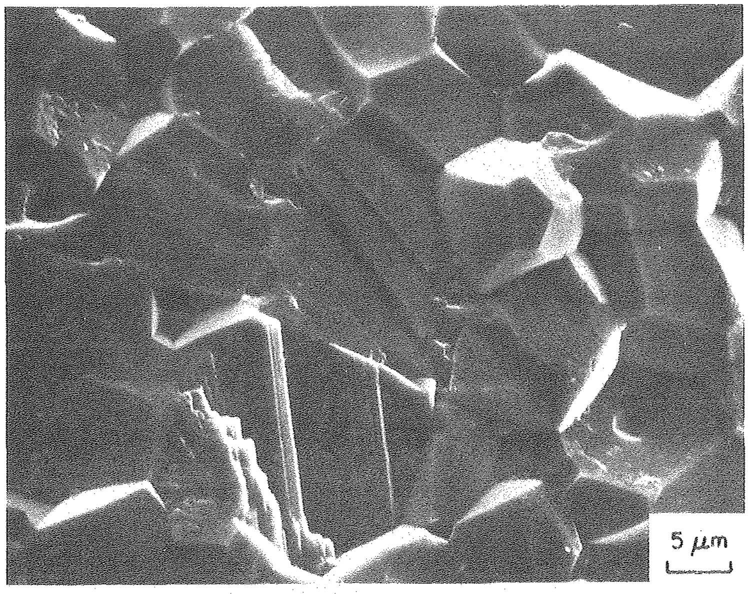

Fig. 4.15. Fracture surface. The steps are indicative of transgranular fracture which has followed crystallographic directions.

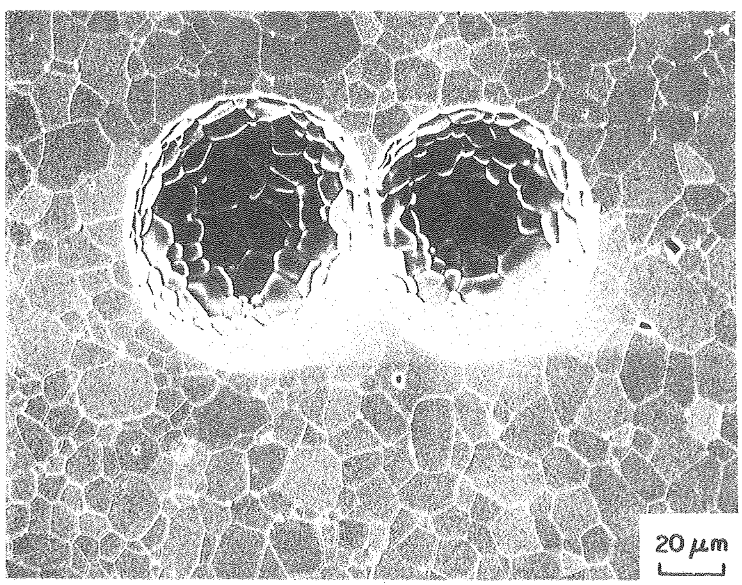

Fig. 4.16. Polished and etched surface, linking of two voids.

XBB 789-10744

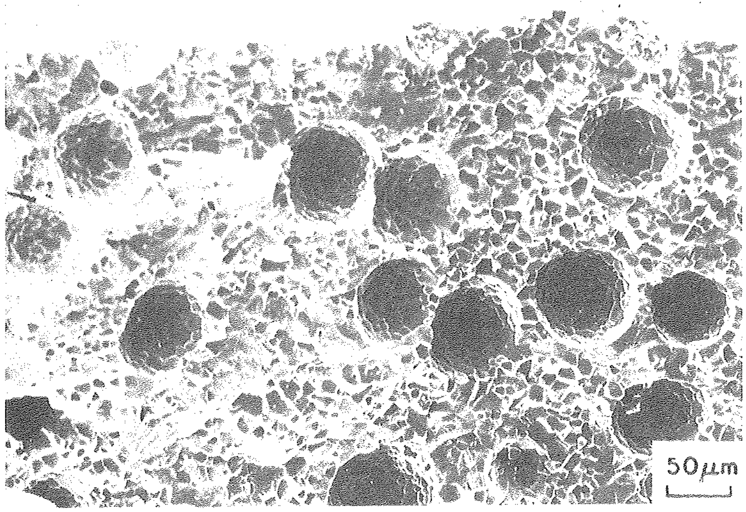

Fig. 4.17. Tensile surface/fracture surface. Large cluster of voids beneath the tensile surface.

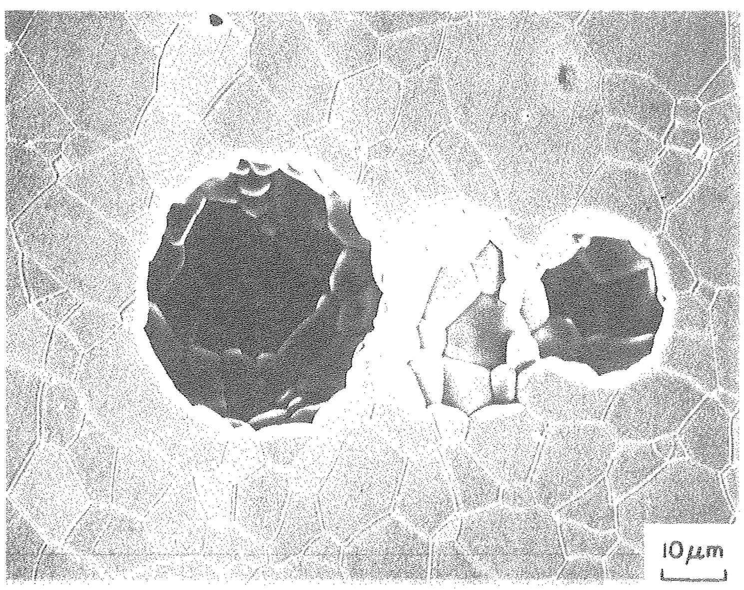

XBB 789-10743

Fig. 4.18. Polished and etched surface. Linking of three voids.

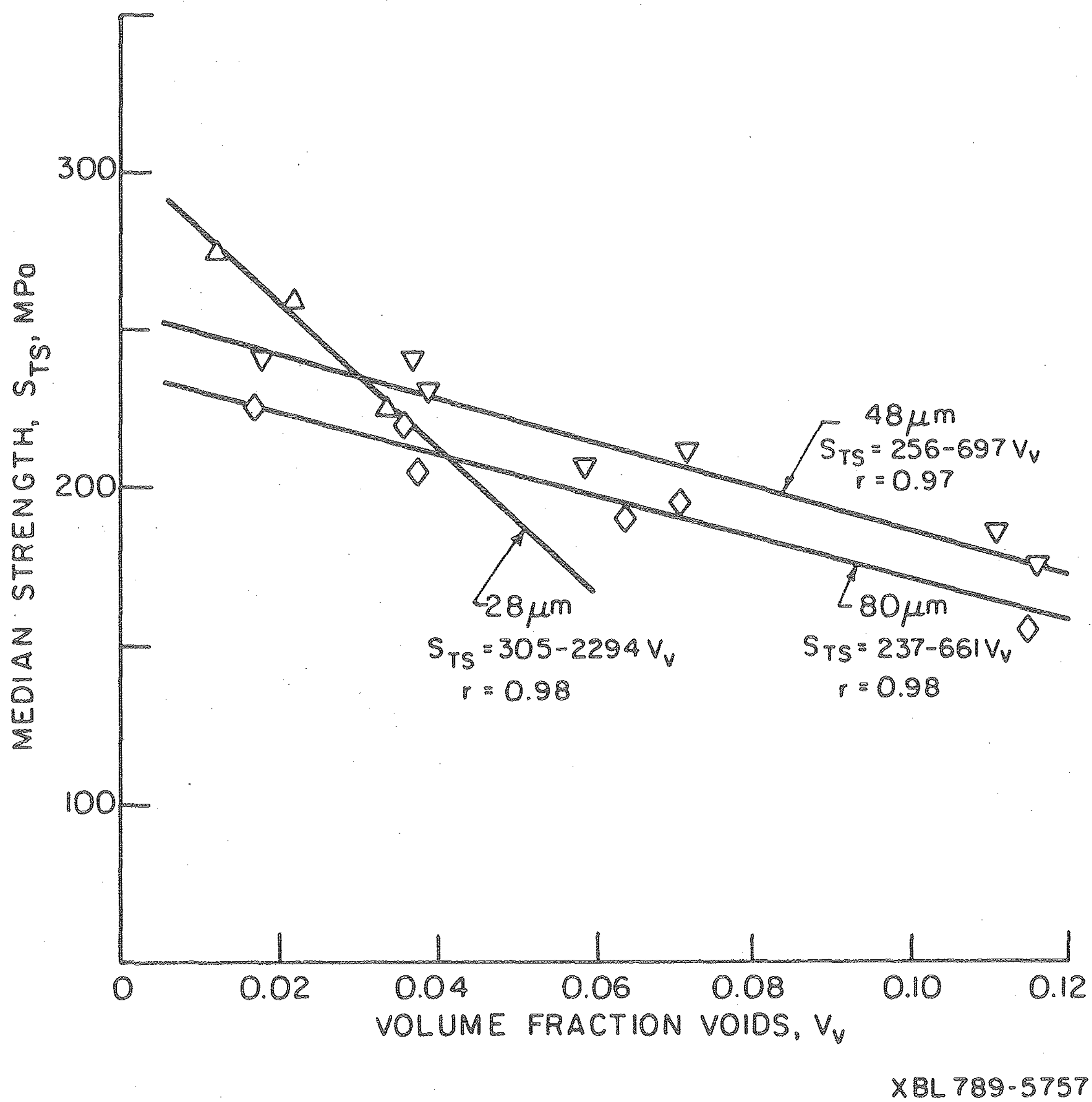
MEDIAN STRENGTH, S_{TS}, MPa
300
200
100
0
0.02
0.04
0.06
0.08
0.10
0.12
VOLUME FRACTION VOIDS, V_v
48 μm
S_{TS} = 256-697 V_v
r = 0.97
28 μm
S_{TS} = 305-2294 V_v
r = 0.98
80 μm
S_{TS} = 237-661 V_v
r = 0.98
XBL 789-5757

Fig. 4.19

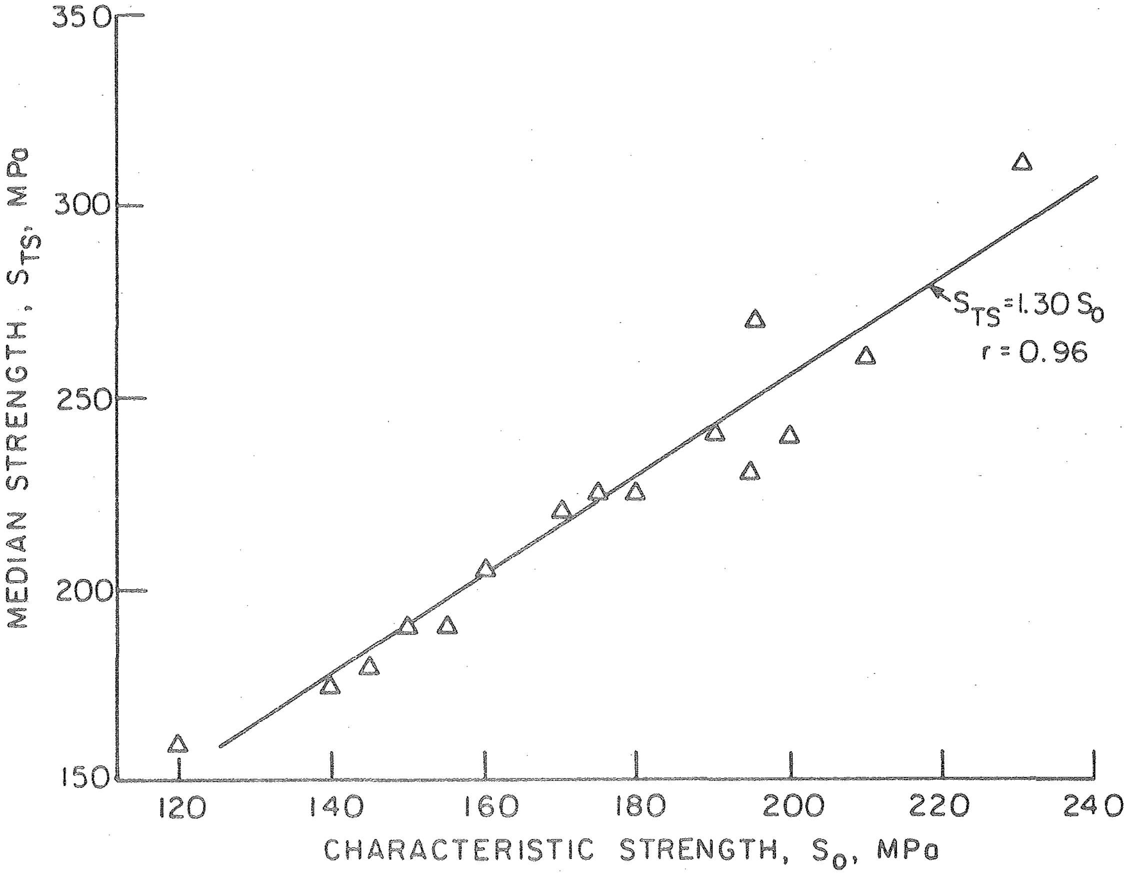

XBL 789-5758

Fig. 4.20

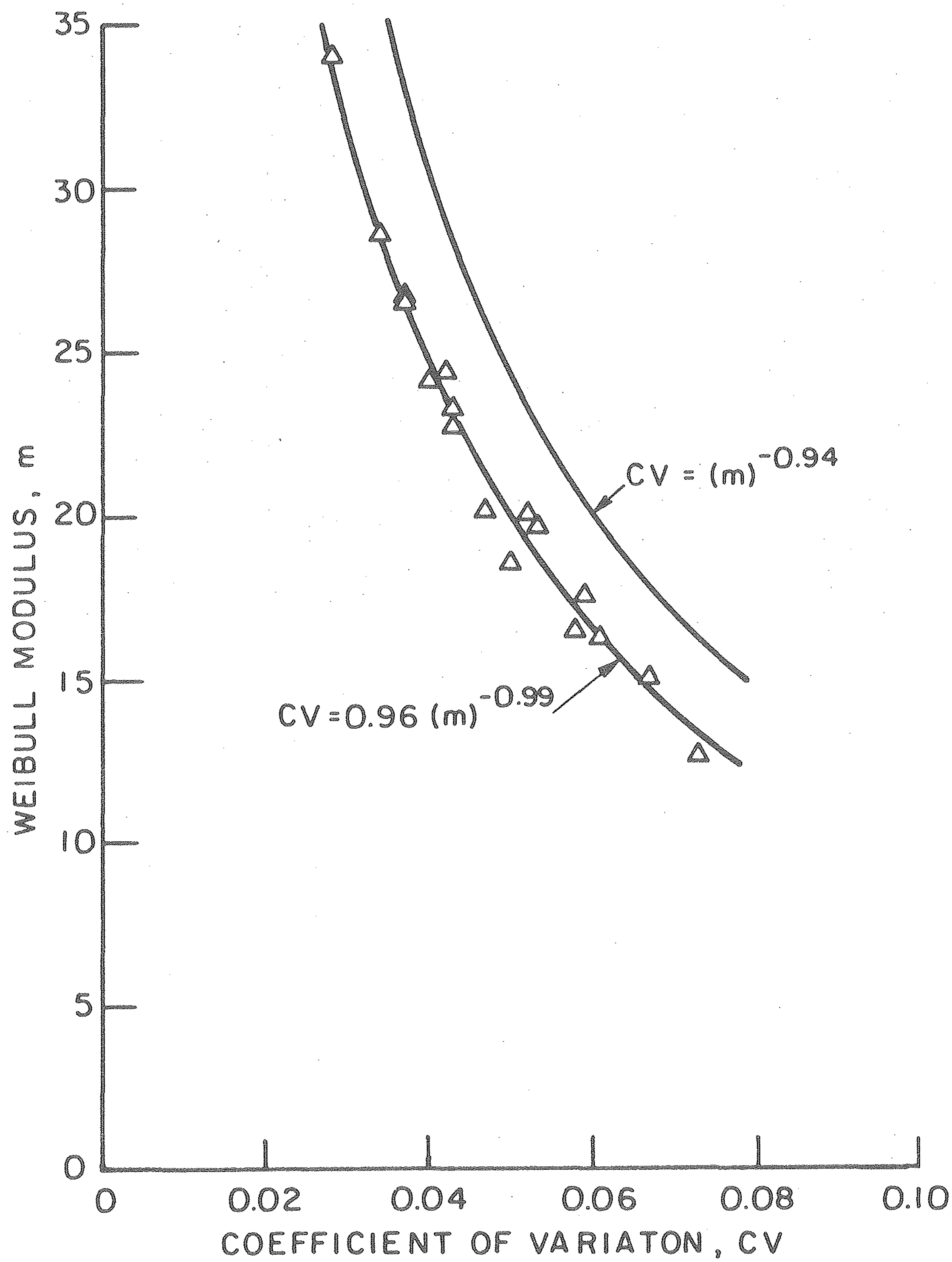

XBL789-5759

Fig. 4.21

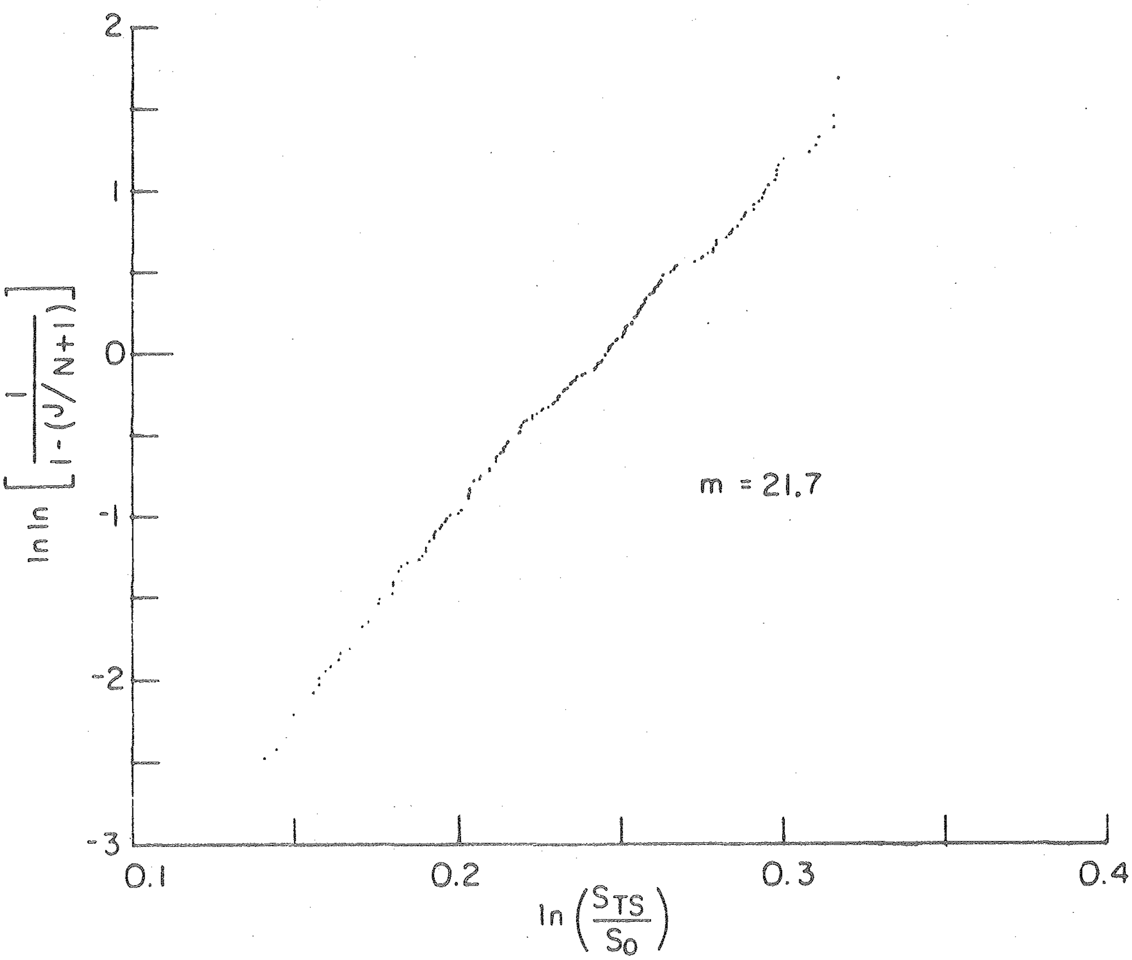

Fig. 4.22

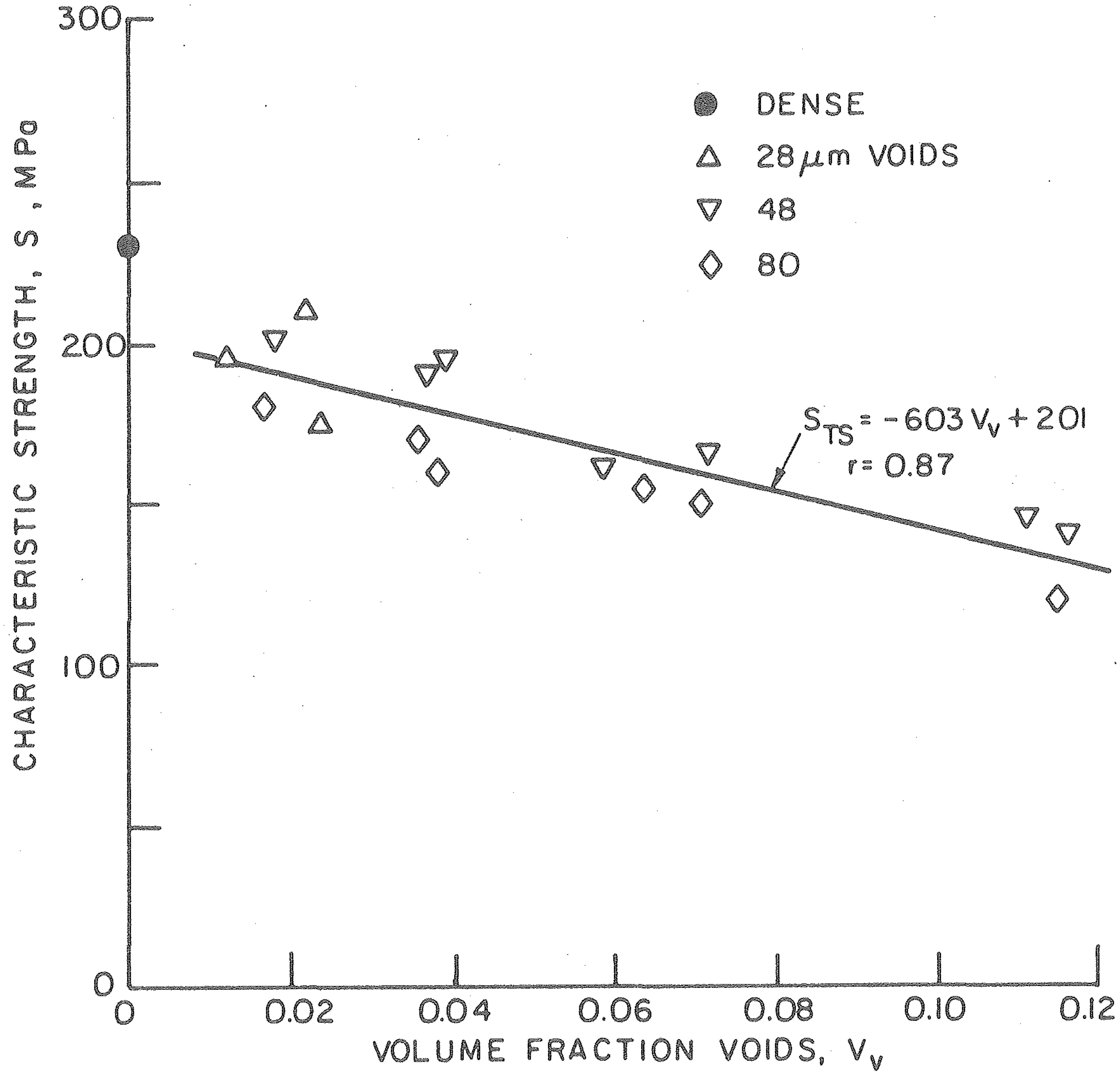

XBL 789-5761

Fig. 4.23

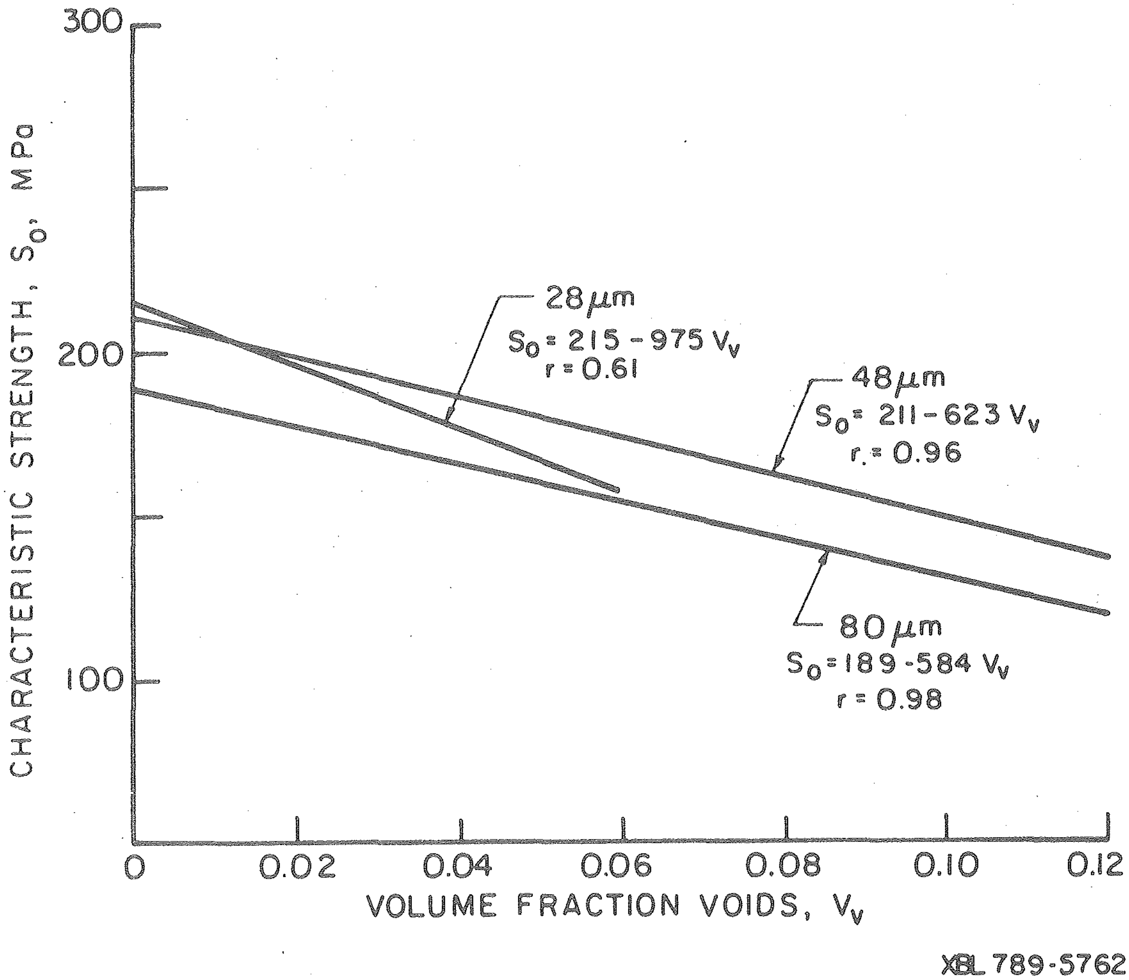
300
200
100
CHARACTERISTIC STRENGTH, S_o, MPa
28 μm
$S_o = 215 - 975\ V_v$
r = 0.61
48 μm
$S_o = 211 - 623\ V_v$
r = 0.96
80 μm
$S_o = 189 - 584\ V_v$
r = 0.98
0
0.02
0.04
0.06
0.08
0.10
0.12
VOLUME FRACTION VOIDS, V_v
XBL 789-5762

Fig. 4.24

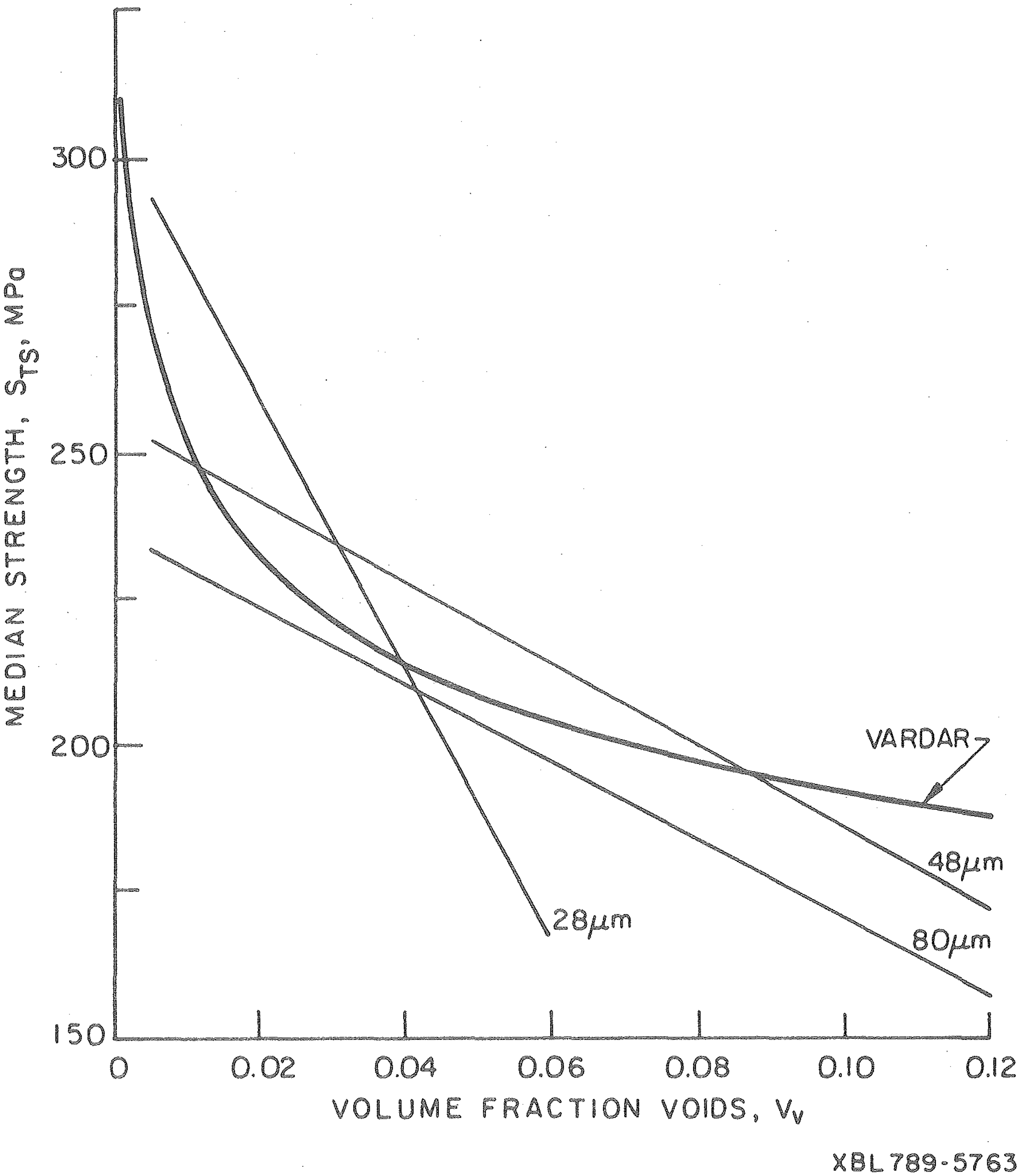
MEDIAN STRENGTH, S_{TS}, MPa
300
250
200
150
0
0.02
0.04
0.06
0.08
0.10
0.12
VOLUME FRACTION VOIDS, V_v
VARDAR
48μm
28μm
80μm
XBL 789-5763

Fig. 4.25

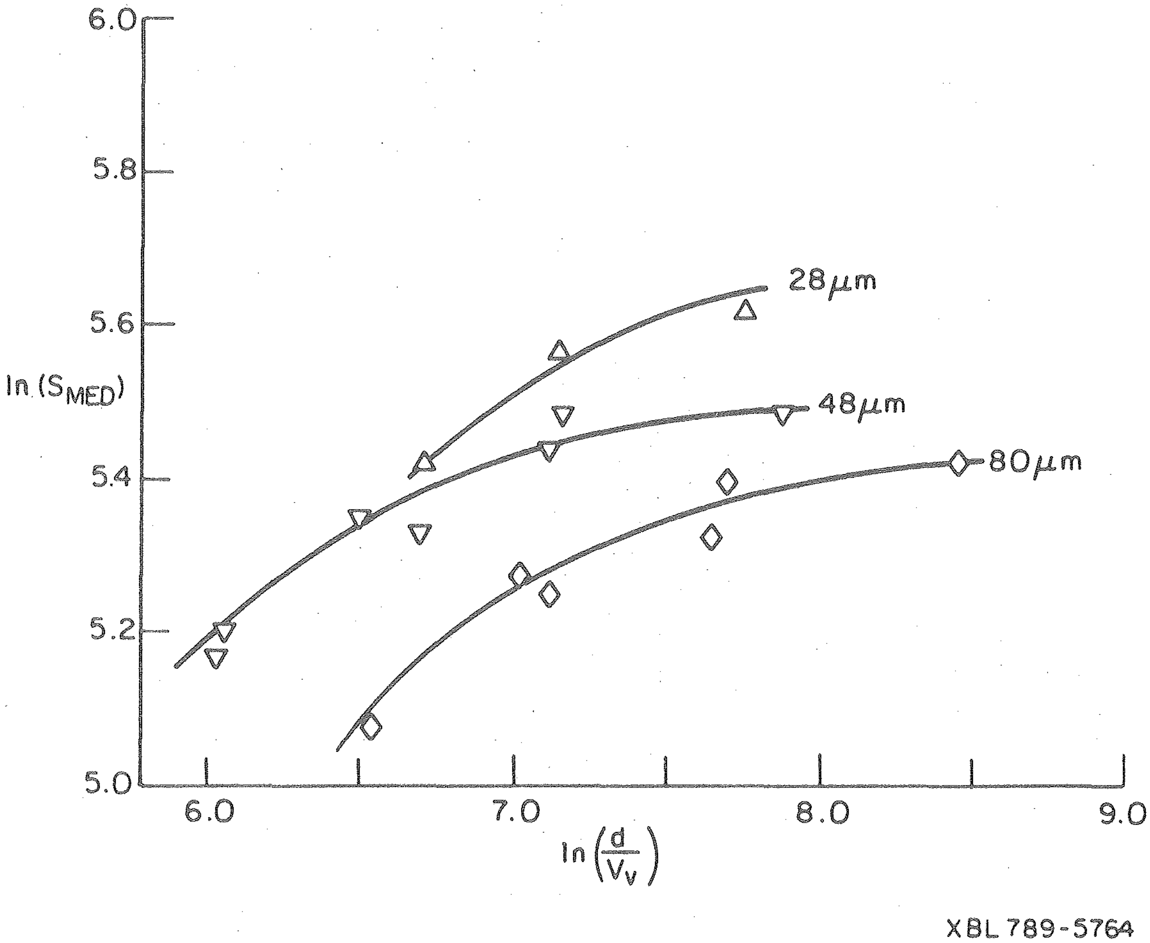
6.0
5.8
5.6
5.4
5.2
5.0
ln (S$_{MED}$)
28μm
48μm
80μm
6.0
7.0
8.0
9.0
ln$\left(\frac{d}{V_v}\right)$
XBL 789-5764

Fig. 4.26

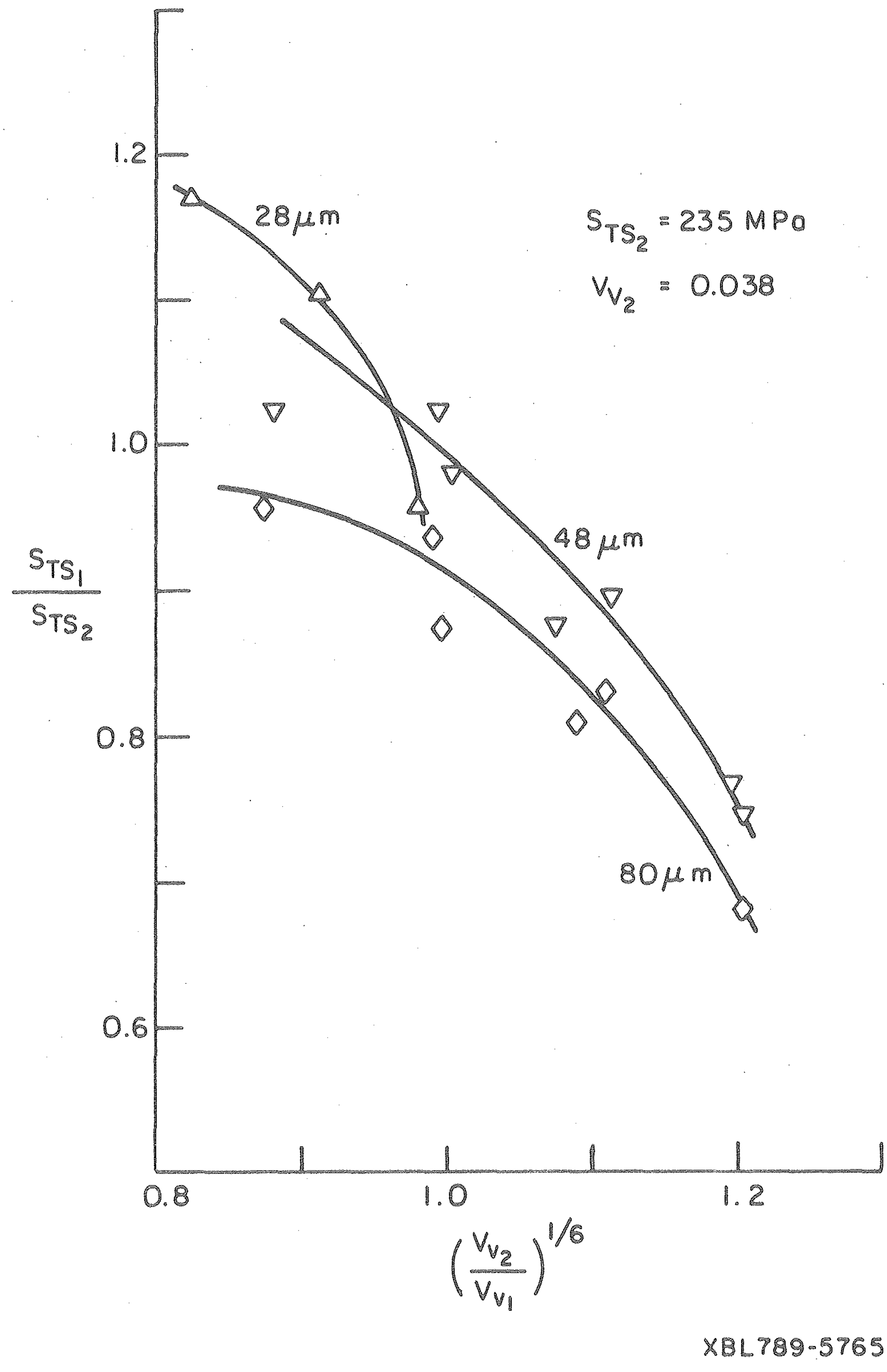

1.2
1.0
0.8
0.6
$\frac{S_{TS_1}}{S_{TS_2}}$
28μm
48μm
80μm
S_{TS_2} = 235 MPa
V_{V_2} = 0.038
0.8
1.0
1.2
$\left(\frac{V_{V_2}}{V_{V_1}}\right)^{1/6}$
XBL789-5765

Fig. 4.27

5. DISCUSSION

We have seen from the preceeding sections that the data of this study, while consistent unto itself, does not correlate well with any of the proposed empirical or phenomenological relationships, extensions of Weibull analysis or microstructural relationships. However, the normalized data when pooled together do fit the Weibull plots very well. These favorable pooling results seem to indicate that all specimens failed from the same flaw populations. The fact that Vardar's modified stress field used in conjunction with the Weibull analysis did not prove fruitful would seem to refute this contention.

One of the basic assumptions on which the Weibull approach is founded is that there is no flaw-flaw interaction. This was assumed because, as noted in section 3.5, correcting for any flaw-flaw interactions is nearly impossible. However, photomicrographs of random polished surfaces and fracture surfaces clearly show evidence of void pairs (Figs. 4.6 and 4.16), void triplets (Figs. 4.12 and 4.17) and void clusters (Figs. 4.5 and 4.18). Since the theory of failure of brittle solids is based on the well founded assumption that the most severe flaw (weakest link) is responsible for the failure strength of the specimen, how can the Weibull plot of the normalized data yield a single curve if it ignores void-void interaction? There seem to be only two possible conclusions which may be drawn:

1. Void-void interaction is unimportant and in no way affects the strength of a specimen.
2. Weibull's analysis works, but for the wrong reasons.

The deviation of these data from Vardar's rigorous extension of Weibull's analysis seems to indicate that Weibull's analysis, at least in classical terms, may be incorrect. This contention is further strengthened by the fact that several investigators, including Batdorf,[9] have found limitations in Weibull's analysis. Furthermore, it would seem improbable that a flaw of such dimensions as a cluster of two or more voids would cause less reduction in strength (be a stronger link in the chain) than some intrinsic flaw which cannot be detected at present. This line of reasoning leads to the belief that conclusion 1 is not correct. What then is the explanation of the fact that Weibull's analysis has successfully predicted data for nearly forty years and has predicted the normalized data of this study so well? We have previously noted that Weibull Statistics are based on extreme value theory. Weibull assumed the statistical variation in the size of single flaws composed the change in flaw severity. McClintock took a different approach. He assumed that all single flaws were of approximately the same size (the length of one grain) and that the extreme value of these local single flaw densities leads to the most severe flaw. That is, the most severe flaw consists of 1,2,3,...n single flaws randomly combined to form a large flaw. In the case of externally produced voids a similar situation exists; local variation in void densities produce clusters of voids which may be considered as the large flaw. As noted by Pankow,[19] Weibull and McClintock are compatible within the normal range of experimental data (volumes), thus it is not unreasonable for our normalized data to fit Weibull Statistics. It is the author's opinion that

McClintock's "simple and inexact model" of randomly combined single defects provides a sound explanation of the strength behavior of polycrystalline brittle solids. The fact that the McClintock model predicts forty years of data as well as does Weibull's analysis lends some credence to this opinion.

6. CONCLUSIONS

In this study we have examined the effect of artificially introduced voids on the strength of a polycrystalline brittle solid. Traditional empirical and phenomenological strength-porosity relationships were found to correlate poorly with the data.

The most possible direct test of Weibull Statistics using Vardar's analysis of the stress field produced by spherical voids indicated that these data did not follow Weibull Statistics. Based on microstructural examination, Weibull's basic assumption of no flaw-flaw interaction was shown to be unacceptable in a system of randomly distributed flaws. However, the composite Weibull plot of the normalized strength values indicated that the same flaw populations caused failure in most samples.

Based on McClintock's model of randomly distributed cracked grain boundaries, the weakest link theory and microstructural evidence of clusters of voids, we propose that fluctuations in the local void densities produce clusters of voids which are the most critical flaws in the sample and are thus responsible for the noted reductions in strength with increasing void fractions.

ACKNOWLEDGMENT

I must express my sincere appreciation to Professor Joseph A. Pask for his continued involvement and encouragement during the course of this work. Further thanks must be given to Iain Finnie and David Pankow for their worthwhile technical input. I also wish to mention those who not only became technical advisors but also friends — Richard M. Fulrath, Bob R. Powell, Jr., Dipak R. Biswas and Hans Eckart Exner. Many others should be included in any mention of those who have made the last two years at Berkeley so enjoyable and worthwhile but the space is too short for a complete list; those people, students and lab personnel, must be content with the fact that I treasure these two years of my life and will never forget them. Finally, mention must be made of those who provided a warm and loving atmosphere away from the lab — my parents, Mr. and Mrs. A. G. Wallace, and Gwen Tatsuno.

This work was supported by the Division of Materials Sciences, Office of Basic Energy Sciences, U.S. Department of Energy.

Table I

Mean void diameter d, m	Volume Fraction voids, V_v	Mean strength $\bar{S}_{TS}$, MPa	Coefficient of variation CV ($S_o/\bar{S}_{TS}$)	Median strength S_{TS}, MPa	Characteristic strength S_o, MPa	Weibull modulus, m	Number of specimens
-	0	300	0.061	310	230	16.3	11
	.012	270	0.073	275	195	12.7	9
28	.022	255	0.037	260	210	26.6	12
	.034	230	0.067	225	175	15.1	12
	.018	240	0.034	240	200	28.6	12
	.037	235	0.043	240	190	23.3	13
	.039	235	0.029	230	195	34.2	11
48	.059	205	0.052	205	160	20.0	12
	.072	210	0.047	210	165	20.2	9
	.111	185	0.042	185	145	24.4	13
	.116	175	0.043	175	140	22.7	12
	.017	225	0.040	225	180	24.2	10
	.036	215	0.053	220	170	19.7	13
	.038	210	0.058	205	160	16.5	12
80	.064	190	0.037	190	155	26.8	12
	.071	195	0.059	195	150	17.6	13
	.115	155	0.050	155	120	18.6	12
			$\bar{x}$=0.048			$\bar{x}$=20.6	Σ=198

APPENDIX 1

Refer to Fig. 3.1b

Increasing moment
end region

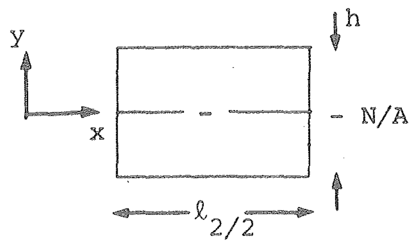

$$\sigma(x,y) = S_{TS}\left(\frac{x}{\ell_{2/2}}\right)\left(\frac{y}{h/2}\right)$$

$$= S_{TS}\ \frac{4xy}{\ell_2 h}$$

$$B_1 = 2\int_V g(S)\,dV = 2\int_V \left(\frac{\sigma(x,y)}{S_0}\right)^m dV$$

$$B_1 = 2w\int_0^{h/2}\int_0^{\ell_2/2}\left[\frac{S_{TS}}{S_0}\left(\frac{4xy}{\ell_2 h}\right)\right]^m dx\,dy$$

$$B_1 = \frac{2w}{(m+1)^2}\left(\frac{\ell_2 h}{4}\right)\left(\frac{S_{TS}}{S_0}\right)^m$$

$$B_1 = \frac{wh\ \ell_2}{2(m+1)^2}\left(\frac{S_{TS}}{S_0}\right)^m$$

Constant moment
center region

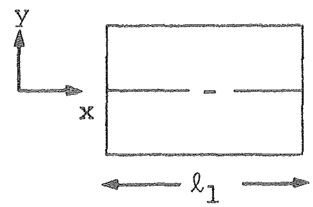

$$\sigma(x,y) = S_{TS}\left(\frac{y}{h/2}\right)$$

$$= S_{TS}\left(\frac{2y}{h}\right)$$

$$B_2 = \int_V g(S)\,dV = \int_V \frac{S_{TS}}{S_0}\left(\frac{y}{h/2}\right) dV$$

$$B_2 = w\ell_1\int_0^{h/2}\left(\frac{S_{TS}}{S_0}\left(\frac{y}{h/2}\right)\right)^m dy$$

$$B_2 = \ell_1 w\left(\frac{S_{TS}}{S_0}\right)^m\left(\frac{h/2}{m+1}\right)$$

$$B_2 = \frac{\ell_1 wh}{2(m+1)}\left(\frac{S_{TS}}{S_0}\right)^m$$

$$B = B_1 + B_2$$

$$B = \left[\frac{wh\ell_2}{2(m+1)^2} + \frac{\ell_1 wh}{2(m+1)}\right]\left(\frac{S_{TS}}{S_0}\right)^m$$

$$B = \frac{wh}{2(m+1)}\left[\ell_1 + \frac{\ell_2}{m+1}\right]\left(\frac{S_{TS}}{S_0}\right)^m$$

REFERENCES

1. O. Vardar, I. Finnie, D. R. Biswas and R. M. Fulrath, Effect of Spherical Pores on the Strength of Polycrystalline Ceramic, Int. J. Fracture 13(2), 215 (1977).

2. J. N. Goodier, Concentration of Stress Around Spherical and Cylindrical Inclusions and Flaws, J. Appl. Mech. 1(1), 39-44 (1933).

3. F. A. McClintock, Statistics of Brittle Fracture, Fracture Mechanics of Ceramics I, Plenum Press, N.Y. (1974), p. 93.

4. R. W. Rice, Fractographic Identification of Strength-Controlling Flaws and Microstructure, ibid, p. 323.

5. O. L. Bowie, J. Math and Phys. 35, 66-71 (1956).

6. A. G. Evans and T. G. Langdon, Structural Ceramics, Prog. in Matl. Sci. Vol.21, Pergamon Press (1976).

7. H. A. Neid and K. Arin, Multiple Flaw Fracture Mechanics Model for Ceramics, Presented at the International Symposium on Fracture Mechanic of Ceramics, July 27-29, 1977.

8. W. T. Koiter, Ingen,Evr ARCH, 28, 168-72 (1959).

9. S. B. Batdorf, Fracture Statistics of Brittle Materials, Nuc. Eng. Des. 35, 349-60 (1975).

10. F. I. Baratta, Stress Intensity Estimates of a Peripherally-cracked Spherical Void and a Hermispherical Surface Pit, Presented at the American Ceramics Society Annual Meeting, 1978.

11. American Society for Testing and Materials STP 381 (1965).

12. A. G. Evans and G. Tappin, The Effects of Microstructure on the Stress to Propagate Inherent Flaws, Proc. Brit. Ceram. Soc. N20 275-97 (1972).

13. G. C. Sih, Handbook of Stress Intensity Factors, Inst. Fracture and Solid Mech., Lehiglt Univ. (1973).

14. H. Tada, The Stress Analysis of Cracks Handbook, Del Research (1973).

15. D. Nk. Wang, (Ph.D. thesis), University of California, Berkeley (1976).

16. Underwood, Quantative Stereology, Addison-Wesley, 1970.

17. J. S. Wallace, unpublished Research

18. R. W. Rice, Fractographic Identification of Strength Controlling Flaws and Microstructure, Fracture Mechanics of Ceramics V1.

19. D. Pankow, The Size Effect in Statistical Fracture, Ph.D. thesis, University of California, Berkeley

20. A. Salak, V. Miskovic, E. Dudrova and E. Rudnayova, The Dependence of Mechanical Properties of Sintered Iron Compacts Upon Porosity, Powd. Met. Int. 6, (2) (1974).

21. I. Finnie, Mechanical Engineering 225B Course Notes, Fall 1976.

22. D. R. Biswas, The Influence of Porosity on the Mechanical Properties of Lead-Zirconate-Titanate Ceramics, Ph.D. thesis, University of California, Berkeley, (1976).

23. I. Finnie, D. Pankow (private communications).

24. R. L. Coble and N. M. Parikit, Fracture of Polycrystalline Ceramics, in Fracture V8 edited by H. Likbowitz, Academic Press 1972.

25. W. D. Kingery, H. K. Bowen and D. R. Uhlmann, Introduction to Ceramics, John Wiley & Sons, 1976.

NOMENCLATURE

a	Half crack length
B	Risk of Rupture
c	constants
CV	coefficient of variation
d	void diameter
G	grain size
g(S)	volumetric strength Function
h	thickness of specimen
H(m),	results of an integration (Vardar et al.)
j	Rank of a specimen (j=1 indicates weakest)
K_{IC}	critical stress intensity factor, mode I
ℓ_1	Distance between inner pivots in 4-point tester
ℓ_2	Twice the distance between the inner and outer pivots in 4-point tester
m	Weibull modulus
N	Number of specimens tested
n	Number
N_{GB}	Number of grain boundaries interesting voids per unit volume
N_v	Number of voids per unit volume
P_s	Probability of survival
r	Correlation coefficient
S	applied stress
S_o	Characteristic strength
S_{med}	Stress an the tensile surface for the median strength specimen

S_{TS}	stress at the tensile surface
$S_{TS(0)}$	S_{med} for $V_v=0$
ν	Poisson's ratio
V	Total stressed volume of a specimen
V_v	Volume fraction of voids (void fraction)
w	width of specimen
Y	constant dependent on flaw geometry and loading conditions